Metavalent multicenter bonding in pnictogens and chalcogens: nature and mechanism of formation

Hussien H. Osman[1,2,3*], Alberto Otero-de-la-Roza[4], P. Rodríguez-Hernández[5], Alfonso Muñoz[5], and Francisco J. Manjón[1*]

[1] Instituto de Diseño para la Fabricación y Producción Automatizada, MALTA Consolider Team, Universitat Politècnica de València, 46022, València, Spain

[2] Instituto de Ciencia de los Materiales de la Universitat de València, MALTA Consolider Team, Universidad de La Laguna, 38205, La Laguna, Tenerife, Spain

[3] Chemistry Department, Faculty of Science, Helwan University, Ain-Helwan, 11795, Cairo, Egypt

[4] Departamento de Química Física y Analítica, MALTA Consolider Team, Universidad de Oviedo, 33006, Oviedo, Spain

[5] Departamento de Física, Instituto de Materiales y Nanotecnología, MALTA Consolider Team, Universidad de La Laguna, 38205, La Laguna, Tenerife, Spain

*Corresponding author(s). E-mail(s): hussien.helmy@uv.es; fjmanjon@fis.upv.es

Abstract

Due to the exceptional property portfolio and technological applications of phase change materials, mostly chalcogens related to IV-VI and V_2-VI_3 families, which are in turn related to pnictogens (group V or 15) and chalcogens (group VI or 16), the nature of the unconventional chemical bonding in these materials has been debated for almost 70 years. This unconventional bond, which has been quoted in the literature as resonant, hypervalent, electron-rich multicenter, three-center-four-electron (3c-4e), and metavalent, is believed to be responsible for the exceptional properties of phase change materials. In the last decade, two bonding models, the metavalent and the electron-rich multicenter models, have competed to explain the nature of this unconventional bond, which we have here renamed as metavalent multicenter bond (MMB) for the sake of clarity. In this comprehensive work, we address the nature of MMB and propose that MMB is an electron-deficient multicenter bond (EDMB), related to the threecenter-two-electron (3c-2e) bond. For that purpose, we explore the pressure-induced mechanism of MMB formation in the some of the simplest possible systems, pnictogens (As, Sb, Bi) and chalcogens (Se, Te, Po), with density-functional theory calculations. In the way, we find that polonium is the only element among chalcogens and pnictogens with crystalline α and β structures already exhibiting MMBs at RP. We find that the mechanism of MMB formation in pnictogens (chalcogens) is comprised of three (two) stages, is similar to that of the EDMB formation in B_2H_6, in some Zintl phases, intermetallics, and cluster compounds, and in atomic/polymeric nitrogen and hydrogen at high pressures. On the other hand, the mechanism of EDMB formation is completely different from that of the 3c-4e bond formation in molecules. Finally, we propose the simplest geometries of EDMBs that can be found in solids along one, two, and three dimensions and comment on the validity of the doublet/octet rules in the hypercoordinated multicenter units with EDMBs.

1. Introduction

The concept of chemical bond is commonly used to understand key features of the structure and properties of molecules and solids. The prototypical bonding types, like covalent, ionic, and metallic bonds, are widely discussed in the textbooks; however, several other interactions, including hypervalent, donor-acceptor, pnictogen, chalcogen, halogen, and multicenter bonding, have also been found beyond such idealized bonding descriptions [1–3]. Since the chemical bond is an elusive and controversial concept because it is not directly given by a quantum-mechanical operator[4,5], several approaches have been developed over the last few decades to analyze the different types of chemical bonding in solids based on quantum-mechanical wavefunctions and electron densities. In this regard, chemically meaningful entities, such as bonding electron pairs (Lewis pairs) and lone electron pairs (LEPs), can be analyzed using natural bond orbitals [6], Wannier functions [7,8], electron localization function (ELF) [9], and the chemical-pressure formalism [10,11], among others.

A great deal of attention has been recently devoted to the analysis of the chemical bonding in phase change materials (PCMs) consisting of binary chalcogenides of the IV-VI and V_2-VI_3 families, such as GeTe, SnTe, Sb_2Te_3, and their related ternary compounds, such as $Ge_2Sb_2Te_5$ (GST). PCMs have an exceptional *property portfolio* that includes: i) hypercoordination (violation of the 8-*N* rule); i.e. a higher atomic coordination than expected for compounds with covalent *ppσ*-bonds that do obey the 8 − *N* rule, ii) relatively low band gaps and shiny metallic luster, iii) moderate electrical conductivity, iv) extremely high optical dielectric constants and Born effective charges, v) low-frequency optical phonons and high Grüneisen parameters, vi) low thermal conductivity, and vii) brittleness and high probability of multiple emission events in laser-assisted field evaporation measurements, which has been attributed to the softer character of their bonds than of covalent ones [12,13]. Thanks to these unconventional properties, PCMs have a wide range of applications such as re-writable data storage in DVDs, phase change RAM memories, and thermal energy storage systems [14–17]. Moreover, many PCMs also show highly efficient thermoelectric and exceptional topological properties [18–20]. Until the last decade, the unconventional chemical bonding in PCMs was considered to be a kind of resonant bonding related to the single covalent (two-center-two-electron, 2c-2e) bond [21–24]. This was similar to that suggested by Pauling for benzene and graphite (latter extended to metals) [25–27] with the possible participation of *d* orbitals. However, from the 1980 decade on, it was noted that: i) the contribution of *d* orbitals to the unconventional bonding in PCMs is minor [28], ii) the influence of *s*-*p* mixing, related to the LEP stereoactivity, in the bonding of PCMs is essential [29–33], and iii) the properties of PCMs are completely different from those of benzene and graphite [13,34].

Although the concept of resonance and resonant bonding has been widely used and discussed to explain the unconventional bonding in PCMs, as recently reviewed [35,36], two alternative chemical bonding models have rivaled for explaining their exceptional properties in the last decade. On the one hand, several groups, including Kolobov and coworkers [37,38], Dronkowski and coworkers [39–41], and Lee and Elliot [42–44] have considered that PCMs feature electron-rich multicenter bonds (ERMBs). The ERMB is considered to be the generalization and extension of the three-center-four-electron (3c-4e) bond, proposed by Rundle and Pimentel for molecules, such as I_3^- and XeF_2 [45,46], and that is also related to the concepts of donor-acceptor bonds

[47] and hypervalent bonds [48–51]. In particular, Dronkowski and coworkers demonstrated the electron delocalization and multicenter character of bonding in PCMs by calculations of the projected force constants along several atoms and of the crystal-orbital bond index (COBI), together with its integrated values for two-center and three-center bonds, ICOBI(2c) and ICOBI(3c), respectively [39–41]. The multicenter character of bonding in PCMs has also been recently justified on the basis of a three-center "covalent-like" interaction [52].

On the other hand, Wuttig and coworkers have proposed that PCMs feature a new unconventional bonding characterized by a mixture of localized electrons (as in covalent materials) and delocalized electrons (as in metals); i.e. a bond that is intermediate between the 2c-2e bond and metallic bonds and is argued to be a kind of two-center-one-electron (2c-1e) bond [12,13,34]. Consequently, these authors coined the term "metavalent" bond and considered the materials with this bond as incipient metals. Interestingly, they located incipient metals in an intermediate position between covalent and metallic materials in a 2D map showing the number of electrons shared (ES) vs. the normalized number of electrons transferred (ET), which are defined using Bader's integrated atomic charges and delocalization indices from the Quantum Theory of Atoms in Molecules (QTAIM) [53].

The two alternative chemical bonding models for PCMs have been recently reviewed [36] and it has been concluded that both metavalent and ERMB models describe the same bonding scenario. Both models agree that some electrons are localized, i.e. shared between two atoms, and some are delocalized. The two models also agree that the unconventional bonding in PCMs is characterized by sharing less than two electrons per atom pair. In this sense, supporters of the hypervalent ERMB model assume that the ERMB has only two bonding electrons shared between three centers, as was suggested for the Rundle-Pimentel 3c-4e model [54]. Consequently, Jones has proposed that, although terms like resonant bonding and hypervalent bonding are well extended in scientific literature and the term metavalent bonding has become popular in the last five years, the unconventional bonding in PCMs should be called electron-rich multicenter bonding [36] since the existence of multicenter bonds was already postulated in the early days of quantum mechanics [55–57].

In 2023, the two current bonding models of PCMs have been defended by their supporters [58,59]. On one hand, Wuttig and coworkers [58] have suggested that metavalent bonds cannot be ERMBs, as suggested by Jones [36]. Wuttig and coworkers have calculated the ES value between two atoms, as two times the delocalization index [53], in molecules with well-known hypervalent ERMBs or 3c-4e bonds, such as XeF_2 and SF_4 molecules, and have evidenced that they present ES values between 1.5 and 2, i.e. similar to those of covalent bonds. This result differs from the ES values obtained for materials with metavalent bonding (ES ≈ 1), so they have shown that molecules with ERMBs are located in a different position than incipient metals in Wuttig's ES vs. ET map [58]. In this respect, Wuttig and coworkers left open the door for metavalent bonds to be equivalent to charge-shift bonds [60], or even to electron-deficient multicenter bonds (EDMBs). In particular, EDMBs are akin to three-center-two-electron (3c-2e) bonds present in boranes [54,61] and in solids, such as boron [27], boron-based compounds [62], intermetallics [63], and some aluminosilicates [64]. Contrarily, Jones *et al.* [59] insisted that metavalent bonds are indeed ERMBs and that the ES value is not a good parameter to describe

the unconventional bonding in PCMs. These authors argue that the Wuttig's ES vs. ET map is not useful for materials with different kinds of bonds in their crystalline structures [44], e.g. the case of the amorphous phases of PCMs and of crystalline IV-VI and V_2-VI_3 materials showing a mixture of conventional 2c-2e bonds and unconventional bonds at RP. In summary, the dispute regarding the nature of the unconventional bonding in PCMs is unresolved.

It must be stressed that supporters of the two different bonding models in PCMs usually work with different methodologies, which explains in great part their conflicting views. Researchers working with the metavalent bonding model have mainly adopted a phenomenological view and focused on the different properties of the materials, such as electrical and thermal conductivity, optical dielectric constant, Born effective charges, and phonon anharmonicity. Moreover, they used the QTAIM methodology to analyze the topology of the electron density and evaluate the ES and ET values [12,13,24,34,65–69]. Alternatively, researchers supporting the ERMB model have paid more attention to the projected force constants between atoms, the chemical interactions between LEPs and antibonding orbitals σ* of covalent *ppσ*-bonds and the associated electronic band structure of the materials [29,39–44]. These researchers have analyzed chemical interactions through the charge density, ρ, and its Laplacian, $\nabla^2\rho$, at bond critical points (BCPs), the electronic density of states (DOS), the ELF, the crystal-orbital overlap population (COOP), the projected crystal-orbital Hamiltonian population (pCOHP) along the different bonds between two atoms and its integrated value, IpCOHP(2c), and COBI (including ICOBI(2c) and ICOBI(3c)). Furthermore, the supporters of the ERMB model have proposed an explanation for the linear bonding configurations present in PCMs on the basis of the valence shell electron repulsion (VSEPR) theory [43,44]. They have classified the molecular units in amorphous and crystalline phases of GST depending on whether they violate or not the octet rule; the molecular units obeying the octet rule are composed by pure ordinary covalent bonds and LEPs and those violating the octet rule are composed by at least one ERMB in addition to other possible covalent bonds or LEPs [43,44].

In view of the present controversy regarding the nature of the unconventional bonding in PCMs and the merits of the two current bonding models, we will name hereafter this unconventional bond as "metavalent multicenter bond (MMB)". In this manuscript, we try to understand the nature of MMB and show in section 4 that *MMBs are equivalent to EDMBs*. However, it must be noted, before addressing the above issue, that dispute regarding the two bonding models in PCMs started much earlier than shown in the preceding paragraphs. With the change of the millennium, Hoffmann and coworkers studied several Sb-based molecules and compounds with linear bonds in one (1D), two (2D), and three dimensions (3D) [49,50]. In particular, they suggested that the simple cubic (*sc*) phase of Sb should show ERMBs [51]. This is in line with the views of Kolobov and coworkers [37,38], Dronkowski and coworkers [39–41], Lee and Elliot [42–44], and Jones [36,59], and against the position of Wuttig and coworkers, who considered that this phase (*sc*) of a single element (Sb) shows the same metavalent –previously resonant– bonds as PCMs [69–71]. Similarly, Lubchenko and coworkers reported the presence of multicenter bonds in Bi_2Te_3 [31], unlike Wuttig and coworkers, who later considered the presence of metavalent bonds in all tetradymite-like V_2-VI_3 chalcogenides [68]. In other words, the dispute regarding the nature of the unconventional bonding in PCMs and in octahedrally-coordinated

pnictogens goes beyond the two current research teams that have supported their claims in 2023.

Remarkably, Hoffmann and coworkers [50,51] came up with the idea that MMBs in materials, such as *sc*-Sb, had their origin in secondary bonds or backbonds [72], i.e. bonds present in rhombohedral Sb at room pressure (RP) and, in general, in materials showing covalent *ppσ*-bonds in which the participation of LEPs is important. We consider that to understand the MMB nature in *sc*-Sb and in PCMs it is essential to realize that the above consideration suggests that there is a mechanism for the MMB formation in *sc*-Sb. This mechanism involves the transformation of the original primary covalent bonds and secondary bonds into new MMBs. Moreover, Hoffmann and coworkers suggested that secondary bonds, also known as donor-acceptor bonds, charge-transfer bonds [47], or σ-hole bonds [73,74], are similar if not equal to ERMBs/MMBs [49]. Nowadays, several types of secondary bonds, such as hydrogen, triel, tetrel, pnictogen, chalcogen, and halogen bonds, are considered just different types of σ-hole bonds in line with Hoffmann's view [75–79]. Secondary bonds are, in fact, one of the workhorses in supramolecular chemistry [80,81], and molecular materials such as polyiodides, which according to Hoffmann have a similar bonding as PCMs, are of renewed interest due to their outstanding properties [82,83]. In this context, it has been reported that it is very difficult to distinguish between the scenario with primary and secondary bonds involving LEPs (pre-MMB scenario) and the scenario with MMBs because secondary bonds and MMBs seem to be the extremes of a single type of interaction with a continuous degree of strength [31,42,50].

A very useful tool to produce continuous degrees of strength is pressure, since it allows altering interatomic distances with much better accuracy and cleanliness than playing with atomic composition. Pressure is the perfect tool to distinguish between the pre-MMB and MMB scenarios. The importance of applying high pressure (HP) to understand the unconventional bond present in PCMs has been highlighted in several works [13,31,34,52]. Unfortunately, the importance of pressure has not been fully exploited despite examples of the pressure-induced MMB formation in IV-VI and V_2-VI_3 chalcogenides, such as GeSe, SnSe, GeTe, and As_2S_3 [84–87], have been published. In particular, it has been shown how the change from the pre-MMB scenario towards the MMB scenario proceeds as octahedral coordination is approached at HP. In this context, it has been stressed that more HP studies, in particular computational ones, are needed to understand the effect of pressure on MMBs, exploring the bond strength-bond length relation in the pre-MMB scenario and how pressure affects the deviation from octahedral coordination in this scenario [88,89]. Notwithstanding, a systematic study of the pressure-induced MMB formation in elemental pnictogens and in IV-VI and V_2-VI_3 chalcogenides has not been undertaken yet.

One way of addressing the controversy regarding the nature of bonding in PCMs would be to study materials at HP from both real (bond) and reciprocal (band) perspectives [90], particularly studying simple *p*-type elements of groups 15 and 16, which show homoatomic/homonuclear linkages, and are much simpler systems than binary and ternary PCMs [91]. In this work, we follow this approach to illustrate the mechanism of MMB formation in materials at HP from the original primary covalent *ppσ*-bonds and secondary bonds (related to LEPs) present in elemental pnictogens and chalcogens at room pressure (RP). The reason to study *p*-type group-15 and -16

elements is that they are LEP-based semiconductors at RP [92] and are the simplest known materials featuring primary covalent *ppσ*-bonds and secondary bonds at RP. In addition, they have been predicted to transform into MMBs at HP as they approach octahedral coordination, such is the case of the HP phase of *sc*-Sb [93]. The crystalline structures of pnictogens and chalcogens at RP display a small atomic coordination that satisfy the 8−*N* rule, except Po, and it is known that the octahedral distortion decreases as pressure increases [51,94,95]. In addition, the crystalline structures of group 15 (As, Sb, Bi) and group 16 (Se, Te) elements at RP are considered Jones-Peierls distorted structures of the octahedrally-coordinated *sc* phase, in the same way as the crystalline structures at RP of most IV-VI and V_2-VI_3 chalcogens (not PCMs) have been considered to be Jones-Peierls distorted structures of the octahedrally-coordinated cubic rock-salt (*rs*) phase present in many PCMs [24,96–98].

This paper is divided into three sections. In section 2, we analyze the effect of pressure on the structural, vibrational, and electronic properties of the crystalline structures of pnictogens (As, Sb, Bi) and chalcogens (Se, Te, Po) using density-functional theory (DFT) calculations, although our results can be extended to the rest of group-15 and -16 elements. Using theoretical bonding descriptors previously used by the proponents of the two current models of MMBs in PCMs, we confirm the MMB formation in these two elemental families as the octahedrally-coordinated crystalline structures are approached at HP, thus showing that pnictogens and chalcongens at HP can help us to understand the nature of the MMB in PCMs. The only exception in our analysis is Po, whose crystalline α and β structures already exhibit MMBs at RP. We will also show that the existence of MMBs in these elements and PCMs is consistent with the most recent Wuttig's 2D map showing ES vs. ET [68,69]; in other words, the ES value and the ES vs. ET map are reasonably good tools for understanding bonds, like MMBs, even in complex materials, such as PCMs, with different kinds of bonds in a given atomic structure. In section 3, we describe the mechanism of the pressure-induced transformation from the pre-MMB scenario to the MMB scenario in pnictogens and chalcogens using both the real-space (bond) and the reciprocal-space (band) pictures. We will show that the mechanism of MMB formation is similar for pnictogens and chalcogens and proceeds through several stages, which are different for both elemental families. This universal mechanism is expected to apply also to PCMs. In section 4, we address the MMB nature and show that the mechanism of MMB formation in pnictogens and chalcogens (and consequently in PCMs) is similar to that of EDMB formation in diborane and in atomic/polymeric nitrogen and hydrogen phases at HP. This result agrees with the multicenter character previously proposed for MMBs [39–41], but not with the previous hypotheses that metavalent bonding is a new type of bond and that MMBs are ERMBs [58,59]. Our results in fact show that the mechanism of MMB formation is completely different from that of ERMB formation; a result that agrees with Wuttig's claims [58]. Consequently, we propose that MMBs in solids, such as PCMs and pnictogens and chalcogens at HP, are equivalent to EDMBs that are formed in solids, e.g. in Zintl phases, intermetallics, and cluster compounds. Furthermore, we propose the geometries of the hypercoordinated units with EDMBs in solids formed by electron-rich elements, such as group-15 and -16 elements, along one, two, and three dimensions. Details of the *ab initio* simulations for most of the materials studied in this work are given in section 1 of the Electronic Supplementary Information (ESI).

2. Unconventional bonding in group-15 and -16 elements at high pressure

In this section, we perform a systematic theoretical study of the two families of p-type elements at HP, paying special attention to the effect of pressure on the distortion from the octahedral coordination in the trigonal *R*-3m and $P3_121$ structures of group-15 (As, Sb, Bi) and -16 (Se, Te) elements at RP, respectively (Strukturberich types A7 and A8, respectively), as well as on the *P*m-3m (*sc*) and *R*-3m structures of α-Po and β-Po at RP, respectively (Strukturberich types A_h and A_i, respectively). To check the goodness of our theoretical simulations, we have compared the pressure-induced, simulated changes in the structural and vibrational properties of the low-coordinated A7 (As, Sb, Bi) and A8 (Se, Te) phases with available experimental results. The relatively good agreement with experimental results using the PBEsol functional allows us to extrapolate our results to the less well-known HP phases of these two elemental families.

We will prove that unconventional MMBs, as those occurring in PCMs at RP, also occur in the A_h and A_i phases of Po at RP and of As, Sb, Bi, Se, and Te at HP. For that purpose, we calculate several quantum-mechanical bonding descriptors of physical and chemical meaning for the studied phases. In particular, we will use descriptors extensively used by Wuttig and coworkers and Manjón and coworkers [12,13,87,99], such as the optical phonon frequencies, ω_i, and the corresponding Grüneisen parameter, γ_i, which can give evidence of soft bonds and lattice anharmonicity; the average of the diagonal components of the Born effective charge tensor, Z*, which accounts for the bond polarizability, and the ES and ET values, which allow understanding the degree of bond covalency and ionicity, respectively. We will also use other bonding descriptors used by Lee and Elliott, Dronkowski and coworkers, and Manjón and coworkers [39,40,42,87], such as ρ, $\nabla^2\rho$ at BCP, and the pCOHP, IpCOHP(2c), and ICOBI(3c) parameters. These last parameters will help us to describe the evolution of the different atomic interactions as pressure increases. All these parameters, previously used for binary and ternary PCMs, as already remarked, will show us how physical and chemical worlds can be made compatible to provide a richer perspective of the unconventional bonds present in the octahedrally-coordinated phases of pnictogens and chalcogens. More specifically, the existence of MMBs will be evidenced by the small ω_i, soft-mode behavior, and large γ_i for optical phonons, the extremely high values of Z*, and the ES values close to 1. In addition, the existence of MMBs will be confirmed by: i) the very small value of $\nabla^2\rho$ [42,99], which is intermediate between the negative values, typical for the covalent bond, and the positive values, typical for the metallic bond [100]; and ii) a value of ICOBI(3c) different from zero, which gives account for the multicenter character of MMBs [42].

Group-15 elements. The relaxation of the structural parameters of pnictogens (As, Sb, Bi) in the A7 phase at different pressures evidences a decrease in the octahedral distortion of the A7 structure at HP until a final octahedrally-coordinated A_h (*sc*) structure is reached (see **Fig. 1** and **Table S1** in ESI). This is evidenced by the decrease of the quadratic elongation of the distorted octahedron around each atom in the A7 structure and the increase of the effective coordination number (see **Figs. S1c, S2c,** and inset of **S4a** in ESI). In particular, a progressive change in the effective coordination from the trigonally-coordinated A7 structure, characterized by three primary short covalent bonds plus three long secondary bonds (related to LEPs), towards the octahedrally-coordinated A_h structure, characterized by six equal bonds each at 90°, is observed.

These results are consistent with previous expectations and with the observation of the *sc* structure in P and As at HP [101]. The best example is As that has an A7-to-A_h phase transition (PT) theoretically predicted at a transition pressure (P_t) of 25 GPa in good agreement with experimental results (see inset of **Fig. S1a** in ESI) [94]. The theoretically optimized atomic volume and lattice parameters of the As-I (A7) and As-II (A_h) phases at different pressures exhibit a nice agreement with available experimental data [94] and previous calculations [102,103] (see **Fig. S1** in ESI). Remarkably, our structural relaxations of the trigonal A7 phase do not reach the perfect A_h phase except for very high pressures (e.g. our calculations for As just above 25 GPa always show a residual trigonal distortion of the *sc* phase). This result agrees with the most recent and accurate experimental measurements on phosphorous, where a distorted *sc* phase (pseudo-sc) is reported as an intermediate phase between the A7 and the A_h phases [104].

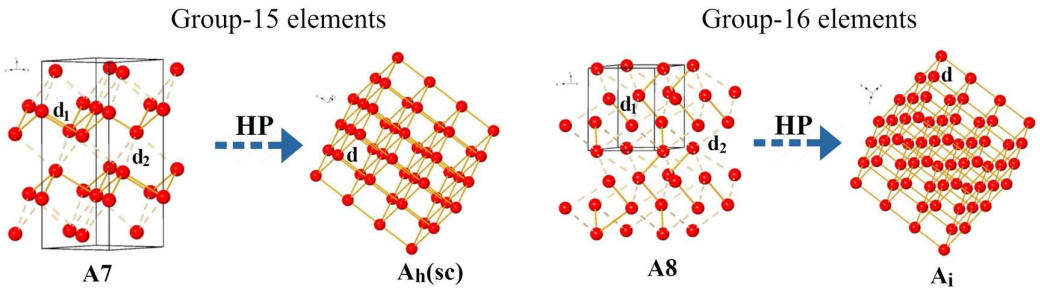

FIG. 1. Phase transition sequence studied in group-15 and -16 elements. Group-15 elements crystallizing in the rhombohedral A7 phase tend at HP to the cubic A_h phase. Group-16 elements crystallizing in the hexagonal A8 phase tend at HP to the rhombohedral A_i phase. The short intralayer (intrachain) d_1 bond distance and the long interlayer (interchain) d_2 bond distance of the A7 (A8) phases in group-15 (16) elements are represented with solid and dashed orange lines, respectively. A_h and A_i phases only feature a single bond distance, *d*.

A characteristic experimental feature of IV-VI and V_2-VI_3 chalcogenides, such as GeSe, GeTe, SnTe, and As_2S_3 that are not PCMs at RP but develop MMBs at HP, is the softening of some optical phonon frequencies at the pre-MMB scenario and hardening of these optical phonon frequencies at the MMB scenario, i.e. a change in sign of the pressure coefficient of the frequency in some optical modes [13,84–87]. A similar feature is experimentally found in As [94] and nicely reproduced by our calculations (**Fig. 2a**). In this sense, the small values of the frequencies of the Raman-active phonons in As at RP (below 300 cm^{-1}) compared to those of Ge (above 300 cm^{-1} [105]) and the soft behavior of the optical phonons of As at HP compared to their increase in Ge [105] prove that the bonds in the A7 structure of As are quantitatively and qualitatively different than those of the zinc-blende structure of Ge. This is contrary to expectations since both elements are close in the periodic table and have similar masses, which could suggest similar phonon frequencies and behaviors.

Curiously, our calculated Raman frequencies for As-I soften at a much higher rate above 10 GPa than the experimental ones, i.e. the calculated Raman frequencies of As-I tend to zero at P_t, unlike the experimental ones. This means that our simulations for As, as the most extensive ones to date by Silas et al. [102]) show soft optical phonons that, according to the Landau theory, correspond to a second-order A7-to-A_h PT. This theoretical result contrasts with the apparent first-order character of the experimental PT [94]. The disagreement could likely be caused by

anharmonic effects that are not included in our simulations. In this context, it is well known that anharmonic effects are notable in PCMs and important for the description of the vibrational properties as the MMB formation is approached [13,52,85,86,106,107]. The presence of strong anharmonic interactions in As-I close to P_t is also evidenced by the large values of the absolute phonon Grüneisen parameter, $|\gamma_i|$, of the A_{1g} mode (inset of **Fig. 2b**). It must be stressed that while optical phonons in PCMs soften upon crystallization, i.e. when MMBs are formed, a hardening of the low-energy acoustic phonons is experimentally observed [106]. The soft (hard) behavior of optical (acoustic) phonons has been also encountered in pnictogens at HP [108,109] and it has been recently understood in the light of a simple model of three-center "*covalent-like*" interactions, which supports the multicenter character of bonds in PCMs, as already pointed out [52].

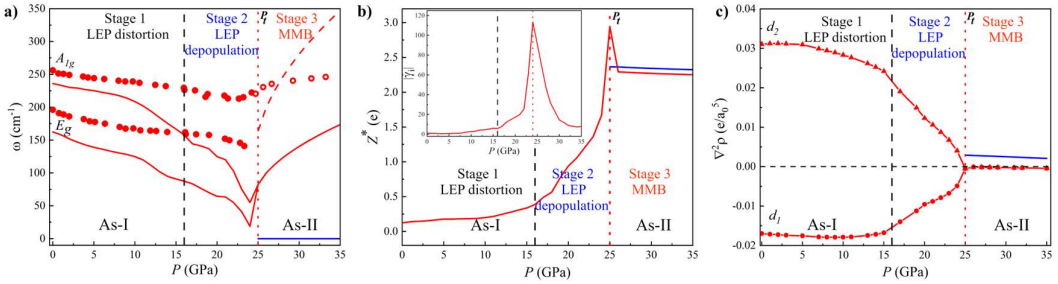

FIG. 2. Pressure dependence of the properties of the As-I (A7, red) and As-II (A_h, blue) phases of As. a) Calculated (lines) and experimental [94] (circles) phonon frequencies, ω, correspond to Raman-active modes A_{1g} and E_g of As-I. Solid and dashed red lines above 25 GPa correspond to first and second-order (overtone) modes of the distorted *sc* phase of As-I, respectively. b) Calculated average Born effective charge, Z*. The inset shows the absolute Grüneisen parameter, $|\gamma_i|$, of the A_{1g} mode of As-I. c) Laplacian of the charge density at the BCP, $\nabla^2\rho$, where *e* is the electron charge and a_0 is the Bohr radius, in primary and secondary bonds of As-I (red) and the MMB of As-II (blue). The three stages of the mechanism of MMB formation are separated by vertical black dashed and red dotted lines. The latter corresponds to the calculated A7-to-A_h phase transition pressure, P_t.

As regards the A_h phase of As above 25 GPa (As-II), it exhibits only acoustic phonon modes (see blue line in **Fig. 2a**); however, our calculations provide non-zero optical phonon modes above 25 GPa (red line) due to the presence of a residual trigonal distortion of the *sc* structure, as already commented. These *forbidden* optical phonons of the A_h phase (also found for the A_h phases of Sb and Bi (see **Fig. S2d and S4c** in ESI) and in the *rs* phase of PCMs [13,52]) seem to be indeed experimentally observed in As-II with a positive pressure coefficient once the MMBs are formed (see open circles in **Fig. 2a**) [94]. The positive frequency pressure coefficient of this mode agrees with our simulations of a second-order phonon obtained as the overtone of the calculated first-order mode (see the dashed red line above 25 GPa in **Fig. 2a**). Therefore, our calculations reproduce the experimental observations and suggest that the experimental phonons in As above 25 GPa might be caused by a distortion of the *sc* structure in As-II, as already reported for phosphorous [104], likely due to an anomalously enhanced second-order Raman scattering, as recently predicted to occur in incipient metals [110].

The presence of MMBs in As-II is not only confirmed by the change of the pressure coefficient of the optical phonon frequencies and the high value of $|\gamma_i|$ near P_t, but also by the high value of Z* (**Fig. 2b**). The high values of Z* (much higher than the nominal valence (0) of pure As) occur near P_t and also in the A_h phase, as it happens for IV-VI and V_2-VI_3 PCMs that are considered to

be incipient metals [13,68]. Additional confirmation of MMB formation in As-II comes from the pressure dependence of $\nabla^2\rho$ along the main bonds in the A7 and A_h phases (**Fig. 2c**). As expected, $\nabla^2\rho$ is negative for the strong primary covalent intralayer bond (d_1 bond distance) and positive for the weak secondary interlayer bond (d_2 bond distance) in As-I. Both $\nabla^2\rho$ values tend to equalize, especially above 15 GPa, until they reach a value close to zero above Pt. Notably, no classic bond is known to our knowledge to have simultaneously a ρ similar to that of covalent bonds (to be later discussed) and a $\nabla^2\rho$ close to zero [111]. This seems only to happen for the MMB, as it was already shown for Sb-Te2 and Sn-Te2 bonds in crystalline $SnSb_2Te$ at RP [99] and for Sb-Te and Ge-Te bonds in crystalline GST [42].

Significantly, the similarity of the MMBs present in *sc*-As and those present in the *rs* phase of IV-VI PCMs can be understood since both are isoelectronic (10-electron) materials [24]. In particular, As and α-GeTe show a rather close behavior because α-GeTe has a layered *R*3*m* structure at RP with primary *pp*σ-bonds and secondary bonds similar to those of As-I. Furthermore, α-GeTe undergoes a pressure-induced PT to the *rs* phase (β-GeTe), with MMBs similar to those of As-II [13,112,113]. It must be stressed that MMBs in As-II, as well as those in β-GeTe, exhibit a hypercoordinated multicenter unit with cubic geometry as that of **Fig. 3c**. In the cubic geometry, three mutually perpendicular MMBs are formed from three original primary covalent *pp*σ-bonds and their secondary LEP-based bonds, in a similar way as already described for crystalline chalcogenides with *rs* structure, such as PbS, PbSe, PbTe, β-GeTe, and GST [37,44].

Following the same strategy as with elemental As, we have simulated the effect of pressure on the A7 phases of Sb (Sb-I) and Bi (Bi-I) (see **Fig. S2 and S4** in ESI). As already mentioned, the A7 phases of Sb and Bi also tend to transform to the A_h phase. Interestingly, this phase has not been observed in Bi at HP, although the monoclinic Bi-II phase is a slightly distorted *sc* phase, and it remains uncertain whether it exists or not in Sb (see discussion in section 2 of ESI). In any case, we have calculated the A7-to-A_h PT in both elements because it provides valuable insight to clarify the nature of the MMB and the various stages of the pre-MMB to MMB transformation discussed in the next sections.

The simulated atomic volume, lattice parameters, and phonon frequencies of Sb-I and Bi-I as a function of pressure show in general better agreement with the experiment than for As-I. These results suggest that anharmonic effects are less pronounced in Sb and Bi than in As although these elements at RP show bonds that are closer to the MMBs than in As, as we will discuss later. Again, the presence of MMBs in the A_h phase in Sb and Bi is confirmed by the change in the sign of the pressure coefficients of the optical phonon frequencies, the high value of $|\gamma_i|$ near P_t, the increase of the Z* in the A7 phase and its high value in the octahedrally-coordinated A_h phase, and by the negligible value of the $\nabla^2\rho$ in the A_h phase. Therefore, despite that the A_h phase could not be experimentally observed in these compounds at HP, it can be concluded that both Sb and Bi tend to exhibit unconventional MMBs as pressure increases and octahedral coordination is approached.

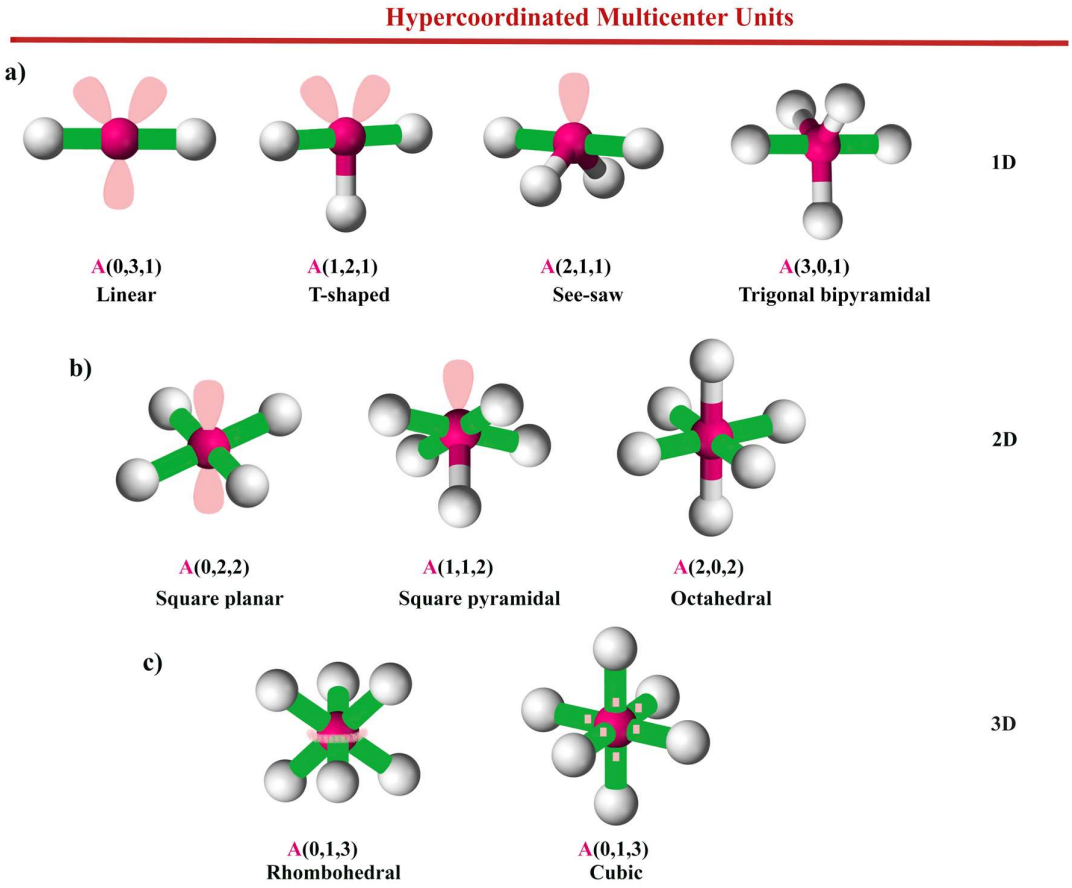

FIG. 3. Hypercoordinated multicenter units around a central electron-rich A atom (pink color) showing the simplest linear three-center bonds in one (1D), two (2D), and three (3D) dimensions. Each unit around the A atom is defined by three numbers enclosed in parentheses, A(C,E,M), denoting the number of covalent bonds (C), LEPs (E), and linear multicenter bonds (M) that are depicted in white-pink, pink, and green color, respectively. These units are typical of molecules with electron-rich multicenter bonds (ERMBs), such as I_3^-, XeF_2, XeF_4, XeF_6, which are also present in molecular solids, such as CsI_3 and Cs_2TeI_6. These units, but extended indefinitely in 1D, 2D, and 3D, also appear in solids with electron-deficient multicenter bonds (EDMBs), such as the octahedrally-coordinated phases of group-15 and -16 elements, in IV-VI and V_2-VI_3 PCMs, such as PbTe and Bi_2Te_3, and in other solids, such as $BaZnSb_2$.

Experimentally, a sign change in the pressure coefficients of the optical phonon frequencies occurs at 25, 9, and 3 GPa in As, Sb, and Bi (see **Fig. S2d and S4c** in ESI for Sb and Bi) [104,114,115]. These results indicate that MMBs are experimentally formed above such pressures. Our simulated P_t values for the A7-to-A_h PT in pnictogens in fact agree for As (25 GPa) and Sb (7 GPa), but not for Bi (14 GPa). Since the P_t value is expected to decrease along the series P-As-Sb-Bi, in agreement with recent experimental results for phosphorous [104], the larger value for Bi than for Sb suggests that PBEsol functional does not work well for Bi. This has been confirmed by lattice dynamics calculations of Bi-I that seem to work well up to 6 GPa, but not above this pressure (**Fig. S4c** in ESI). The reason is the lattice dynamical instability of the the A7 structure above 6 GPa suggested by the presence of imaginary phonons (**Fig. S4e**). Better calculations for Bi-I with the AM05 functional (pink line in **Fig. S4a-c**), which was already used for Bi_2S_3 [116,117], show that compression of the A7 structure results in a monoclinic phase above 2.0 GPa that fully agrees with the experimental observation of the monoclinic Bi-II phase

around 2.5 GPa [101]. In any case, we show hereafter the results obtained with the PBEsol functional for Bi for the sake of comparison with As and Sb under similar conditions.

Since the PBEsol functional works well below 6 GPa, we have simulated the monoclinic phase of Bi-II to be sure about the occurrence of MMBs in the HP phases of Bi. The monoclinic Bi-II phase has a distorted *sc* structure with a very narrow stability pressure range between 2.5 and 2.7 GPa that undergoes a transition to the incommensurately modulated host-guest Bi-III structure above 2.7 GPa (Bi-III is isostructural to Sb-II, the HP phase of Sb above 9 GPa [118]). Our results for the optical phonons of Bi-II at HP (see **Fig. S6** in ESI) show a rather good agreement with experimental results [115,119] and a positive pressure coefficient for all optical modes, as expected once MMBs are formed. On the other hand, the calculated value of Z* in Bi-II shows much larger values than expected for a material with covalent or metallic bonds. Therefore, we conclude that the slightly distorted *sc* phase of Bi-II likely shows asymmetric MMBs, similar to the symmetric MMBs of As-II.

All in all, our calculations on pnictogens show that a bonding change occurs in these elements as pressure increases. The A7 phase at RP features a mixture of primary covalent *pp*σ-bonds plus secondary bonds (related to LEPs), whereas the octahedrally-coordinated HP phases, such as the A_h structure and its slightly distorted structures, feature MMBs that are similar to those already discussed in PCMs, such as IV-VI chalcogenides, which are isoelectronic to pnictogens.

Group-16 elements. Now, we present the results of theoretical calculations of the A8 phase of Se (Se-I) and Te (Te-I) as well as of the A_h and A_i phases of α-Po and β-Po, respectively, at different pressures. As expected, the octahedral distortion, measured by the quadratic elongation of the distorted octahedron around each atom of the trigonal A8 phase in Se and Te, decreases as pressure increases (see **Fig. S7c and S9c** in ESI). However, the relaxation of the A8 structure at HP results in a final octahedrally-coordinated rhombohedral A_i phase instead of the previously assumed cubic A_h phase [24,96,97,120] (see **Table S2** in ESI for the structural parameters of the A8 and A_i phases at different pressures). The A8-to-A_i PT is represented in **Fig. 1**. Our results agree with the experimental observation of the A_i phase at HP in S-V (above 150 GPa [121]), in Se-V (above 40-60 GPa [122,123]), and also in Te-IV (above 10 GPa [124,125]), although the structure of Te-IV has been recently questioned [126]. Therefore, the experimental P_t values for the A_i phase decrease along the series S-Se-Te-Po; a result well reproduced in our calculations for Se (23 GPa), Te (7 GPa), and Po (RP).

The theoretically optimized atomic volume and lattice parameters of the A8 and A_i phases of Se and Te at different pressures exhibit a nice agree with available experimental data and previous calculations (see **Fig. S7 and S9** in ESI) [95,124,125,127–133]. A progressive change is observed in the effective atomic coordination from the twofold-coordinated A8 structure, characterized by two primary short covalent *p*-type bonds plus four long secondary bonds (related to LEPs), towards the octahedrally-coordinated A_i structure of β-Po, characterized by six equal bonds. It must be noted that our structural relaxations of the trigonal A8 phase do not reach the A_i phase of Po at RP, except for very high pressures, so our calculations always show a residual bond distortion of the A_i structure in the pressure range discussed here (see data in **Table 2** of ESI).

Regarding the vibrational properties, both Se and Te exhibit a considerable experimental softening of the A_1 mode of the A8 phase, whose frequency pressure coefficient changes above *ca.* 18 and 7 GPa, respectively [133]. These results are well reproduced by our simulations, except near Pt, where our simulations predict a second-order PT, similar to pnictogens. Again, this disagreement is likely caused by the lack of anharmonic interactions (that seem to be only significant near Pt) in our simulations. The A_i phase does not exhibit optical Raman-active modes (only acoustic phonon modes), but our calculations provide non-zero optical phonon frequencies above 23 GPa in Se and Te (**Fig. S7d and S9d**) due to the remaining distortion concerning the trigonal A_i phase. All the calculated optical phonon frequencies in the distorted A_i phase of Se and Te harden with increasing pressure, as expected once MMBs are formed. As for group-15 elements, the formation of MMBs in the A_i phases of Se and Te is confirmed by the high values of Z* and of the $|\gamma_i|$ for the A_1 mode of the A8 phase (**Fig. S7e and S9e**) as well as by the negligible value of $\nabla^2\rho$ (**Fig. S7f and S9f**). Hence, we conclude that MMBs are formed in Se and Te at HP as they approach the octahedral coordination of the A_i phase.

Remarkably, the bonds in the A_i phase conform to the hypercoordinated multicenter unit with the rhombohedral geometry shown in **Fig. 3c**. In this geometry, three linear multicenter bonds that are not mutually perpendicular are formed from three original primary covalent *ppσ*-bonds and three secondary LEP-based bonds. It must be stressed that the same bond geometry is present in the rhombohedral tetradymite structure of V_2-VI_3 PCMs, such as Bi_2Se_3, β-As_2Te_3, Sb_2Te_3, Bi_2Te_3, and also in the related compound $SnSb_2Te_4$; all of them exhibiting MMBs [12,68,99].

Our theoretical results for Se and Te can be compared with experiments. In particular, several soft phonons still appear in the Se-II and Se-III phases (below 28 GPa) as well as the Te-II phase (below 8 GPa) and similar soft phonons have been observed in amorphous chalcogenides related to PCMs. Since the amorphous phases in chalcogenides, such as GST, are characterized by a mixture of conventional and unconventional bonds with geometries similar to those of the hypercoordinated multicenter units of **Fig. 3a-b** according to the VSEPR theory [44], we also consider that the above-mentioned phases of Se and Te are likely characterized by a mixture of covalent bonds and MMBs with geometries similar to those of **Fig. 3a-b**. Further justification of the geometries described in **Fig. 3** will be given at the end of section 4. The hardening of optical phonons in Se occurs experimentally between 18 and 28 GPa (**Fig. S7d**), i.e. upon transition from Se-II to Se-III, and especially to the Se-IV phase [133]. This change is related to the decrease of resistivity in this pressure region [134]. Similarly, the hardening of optical phonons in Te occurs experimentally above 7 GPa [132,133]; i.e. upon transition to Te-III [124–126,132,133], which is also related to the decrease in resistivity [134]. These changes in Se and Te provide additional support to the presence of asymmetric MMBs in Se-IV (Te-III) as predicted by our calculations above 23 (7) GPa. It must be stressed that the presence of asymmetric MMBs in these intermediate phases of Se and Te, as already suggested to be present in Bi-II, likely occurs before reaching the perfect A_i structure of Se-V and Te-IV phases that are experimentally found at slightly higher pressures.

A paradigmatic example of MMB formation occurs in Po at RP. Po is the only chalcogen that shows octahedral coordination at RP, either in the cubic A_h structure (α-Po) at RP and room

temperature or in the rhombohedral A_i phase (β-Po) at RP and high temperature. Our calculations show that β-Po at RP features a quasi-cubic arrangement of Po atoms, i.e. β-Po shows a very small distortion with respect to α-Po since all six bond distances are equal in both phases and only a small deviation of the rhombohedral bond angle from 90° occurs in β-Po at RP. This deviation disappears at HP, thus leading to a PT to α-Po below 2 GPa (see **Fig. S11** in ESI). As regards the vibrational properties, both phases of Po have only acoustic phonons and the presence of MMBs in Po is here only evidenced by the high (negligible) values of Z* ($\nabla^2\rho$) at all calculated pressures (see **Fig. 4a-b**). Notably, the bonds in α-Po and β-Po correspond to the cubic and rhombohedral hypercoordinated multicenter units of **Fig. 3c**, respectively, already mentioned as possible HP phases of the rest of pnictogens and chalcogens.

All in all, our calculations on chalcogens show that a bonding change occurs in these elements as pressure increases. The A8 phase at RP features a mixture of primary covalent *ppσ*-bonds plus secondary bonds (related to LEPs), whereas the octahedrally-coordinated HP phases, such as the A_i structure and its slightly distorted structures, feature MMBs that are similar to those already discussed in PCMs, such as V_2-VI_3 chalcogenides, which are close to be isoelectronic to chalcogens. Polonium, in its two polymorphs at RP, is the only chalcogen with all bonds being fully MMBs at RP.

Once established that MMBs occur in the octahedrally-coordinated crystalline phases pnictogens and chalcogens either by increasing pressure or by changing composition due to substitution by heavier elements of the same group, we will show next that the change from the pre-MMB scenario to the MMB scenario can be traced by the change of the number of electrons shared (ES) and the normalized number of electrons transferred (ET) in the two-center bonds of materials, as obtained from QTAIM methodology and used by Wuttig and coworkers [12,58,68,69]. As already mentioned, the ES and ET parameters of a two-center bond provide an estimation of the degree of bond covalency and ionicity, respectively.

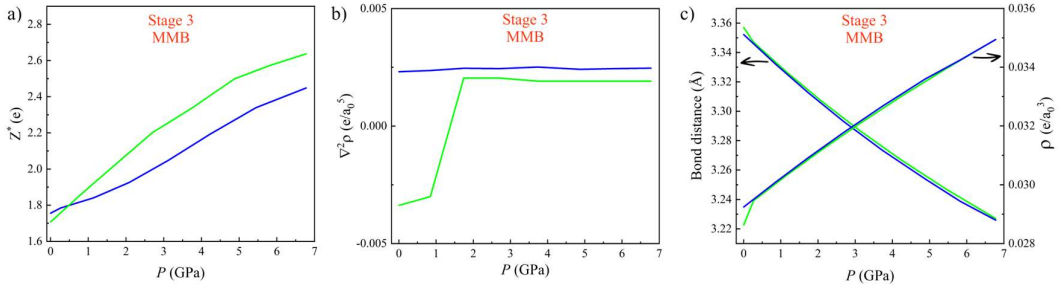

FIG. 4. Pressure dependence of several physical parameters in α-Po (blue) and β-Po (green). a) Average of the diagonal components of the Z* tensor. b) Laplacian of the charge density, $\nabla^2\rho$. c) Bond distance and charge density at the BCP, ρ. *e* is the electron charge and a_0 is the Bohr radius.

In contrast to previous studies, we have calculated the pressure dependence of the ES and ET values in the A7 (A8) phases of group-15 (-16) elements not only for the primary covalent bond (with d_1 length and plotted with solid lines in **Fig. 1**), but also for the secondary bonds of those phases (with d_2 length and plotted with dashed lines in **Fig. 1**). Similarly, we have calculated the ES and ET values of the only bond present in the A_h and A_i phases in these two elemental families. In this way, we can see the evolution of the different bonds as MMB formation proceeds at HP.

Since this work is mainly devoted to pure elements with a unique Wyckoff site at each crystalline structure, the ET values of the primary and secondary bonds are zero; thus, we only need to calculate the ES values of bonds in pnictogens and chalcogens at different pressures. As examples of both families, we show in **Fig. 5** the pressure dependence of ES in As and Se, as well as in α-Po and β-Po. The ES values of the primary covalent bonds in As-I and Se-I at RP are between 1.5 and 2, which are typical of the strong primary covalent bonds, while the ES values of the secondary bonds at RP (around 0.5) are typical of relatively weak secondary donor-acceptor bonds [135]. Remarkably, the ES value of the only bond present in the A_h and A_i phases of As and Se, respectively, is close to 1.0 (once the octahedral coordination is attained in As (Se) above 25 (23) GPa), which is already the value of ES for the two phases of Po at RP. These results mean that the ES values confirm the presence of MMBs in the octahedrally-coordinated phases of group-15 and -16 elements since it is proved that bonds in these phases are characterized by sharing one electron between two atoms, as already suggested by Wuttig and coworkers [58,69]. In other words, MMB in PCMs as well as in the octahedrally-coordinated phases of pnictogens and chalcogens, is a kind of 2c-1e bond. However, it must be stressed that they are not isolated 2c-1e bonds but interacting 2c-1e bonds, as shown by the multicenter character of this unconventional bond [39–41,52].

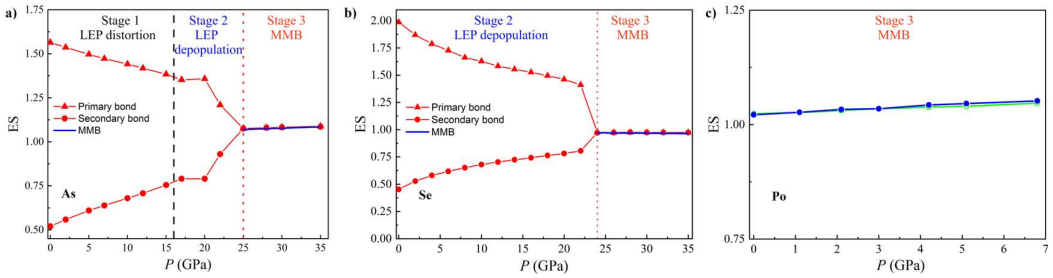

FIG. 5. Pressure dependence of the calculated number of electrons shared (ES) between two adjacent atoms along the primary (triangles) and secondary (circles) bonds in a) As: A7(red) and A_h (blue), b) Se: A8 (red) and A_i (blue), and c) Po: A_h (blue) and A_i (green).

The use of the ES and ET values for primary bonds allows locating the different phases of pnictogens and chalcogens in the 2D map proposed by Wuttig and coworkers to show *metavalency* (see **Fig. 6**) [12,68,69]. As expected, the ES values of the primary covalent bonds in As, Sb, Se, and Te at RP are between 1.4 and 2.0. Meanwhile, the ES value of the primary bond in Bi at RP is 1.2; a value close to 1.0 that corresponds to materials showing MMBs, such as β-GeTe, SnTe, and PbS (PCMs with *rs* structure) [69]. This result shows that Bi is characterized by bonds that are intermediate between covalent bonds and MMBs. This result is consistent with the appearance of asymmetric MMBs in Bi-II above 2.5 GPa (the smallest pressure of all pnictogens), as already commented. Finally, the ES values of the sixfold-degenerated bonds in α-Po and β-Po at RP, as well as in the HP phases of the other elements (As-II, *sc*-Sb, Bi-II, and β-Po phases of Se and Te) are all around 1.0 (see **Fig. 6 and Fig. S12**), thus evidencing that all these phases show MMBs that are in good agreement with their positions in the 2D map [68]. In this context, arrows in **Fig. 6** indicate the direction followed by materials with a mixture of primary covalent bonds and secondary bonds when pressure is applied, or composition is changed for heavier elements within a group.

At this point, it is worth pointing out that MMBs (with ES ≈ 1) are an intermediate step between covalent bonds (with ES ≈ 2) and metallic bonds (with ES → 0), as shown by arrows in **Fig. 6**. This means that MMBs feature an almost equal mixture of localized and delocalized electrons. Since pressure tends to increase atomic coordination, the octahedral coordination will be surpassed at high enough pressures and there will be an increase in the number of delocalized electrons relative to localized electrons. This means that the MMB will tend to become a metallic bond at HP, as suggested by Wuttig and coworkers [13,34]. The tendency of materials with *p*-type bonds to change from covalent bonds towards MMBs and finally to metallic bonds upon the change of pressure or composition is indicated with arrows for pure covalent and ionocovalent *p*-type materials in **Fig. 6**. It can be speculated that the fully metallic bond will occur in pnictogens and chalcogens as well as in IV-VI and V_2-VI_3 chalcogens when the eightfold-coordinated body-centered cubic (*bcc*, Strukturberich type A2) phase is reached, since the A2 phase is a common HP phase to all of them [101,125,136]. This hypothesis seems to agree with the results of Häuserman and coworkers [137], who commented (later discussed) the notable differences between the electronic band structure and DOS in the A2 HP phase and previous phases at lower pressures in Bi. However, the hypothesis of metallic bonding in the *bcc* phase is contrary to the claim of Lubchenko and coworkers, who consider that this phase is still characterized by multicenter bonds [31]. Further work in this direction must be done that is outside the scope of the present manuscript.

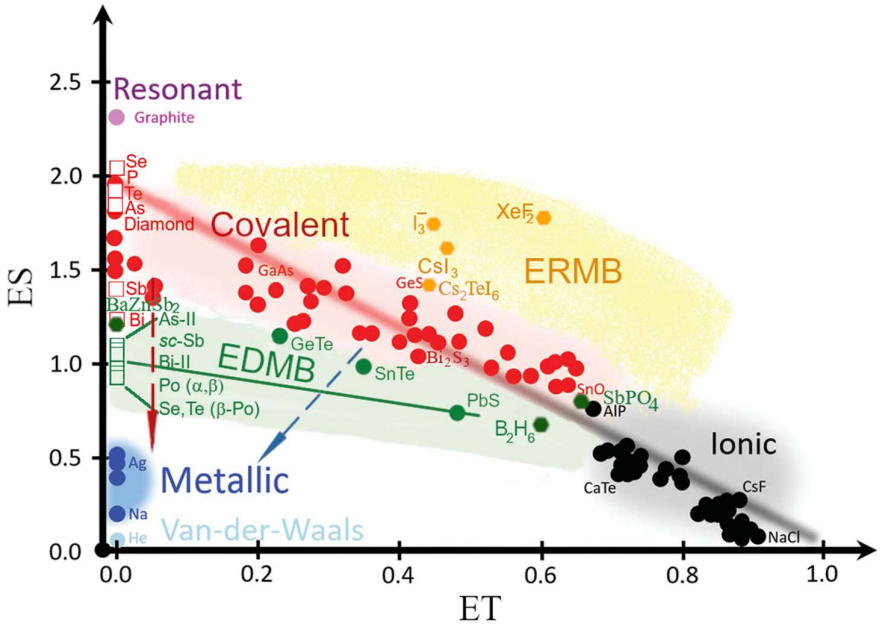

FIG. 6. Revisited 2D map of the number of electrons shared (ES) vs. the normalized number of electrons transferred (ET) showing the chemical bond classification in solids. In particular, the yellow and green regions of materials with electron-rich multicenter bonds (ERMBs) and electron-deficient multicenter bonds (EDMBs), respectively, must be highlighted. MMBs in group-15 and -16 elements as well as in PCMs, such as GeTe, SnTe, and PbS, are located in the region corresponding to EDMBs. Red and blue dashed arrows show the effect of pressure (P) and composition (X) in pure covalent and ionocovalent *p*-type materials, respectively. The studied elements in this work at different pressures are shown as open squares. Other compounds studied here are shown as orange and green hegagons. Reproduced with permission [69]. Copyright 2021, Wiley-VCH.

As already pointed out, a recent paper has suggested that the ES vs. ET map should not be used to understand the origin of MMBs in PCMs [59], because it is impossible to locate in this map materials with more than a single type of bond. This is true and that is why Wuttig et al. only locate materials through their principal bond. We consider that even though the ES vs. ET map cannot be used to univocally characterize materials, it is valid to characterize bonds in materials. We propose that the ES vs. ET map is equivalent to the map already published by Mori-Sánchez et al. to classify bonding types with two parameters, the electron density flatness, *f*, and the global charge-transfer index, *c*, which has been suggested to be equivalent to the van Arkel-Ketelaar diagram [111]. According to our calculations, As-II and α-Po (with *sc* structures) and PbS (with *rs* structure) show *f* values close to 0.1, i.e. intermediate between those of materials with covalent bonding, like Ge and GaAs, and materials with metallic bonding, such as Al and Cu. These results indicate that the region of *metavalency*, intermediate between covalent and metallic regions, can be also placed in the *f* vs. *c* map, and correspondingly in the equivalent van Arkel-Ketelaar diagram. All in all, this means that the ES vs. ET map seems to be equivalent to the *f* vs. *c* map of Mori-Sánchez et al. and the classic van Arkel-Ketelaar diagram. Thus, our results confirm Wuttig's claims that the ES magnitude is valid for locating the *metavalency* region between the covalent and metallic regions [12,13,34]. It must be mentioned that these results differ from those of Lubchenko and coworkers, who suggest that the multicenter bond is only intermediate between ionic and metallic bonds [31]. On the other hand, our results confirm the claim of Lubchenko and coworkers [31] that multicenter bonds are promoted with increasing density since the changes in pressure and in composition (going down within a group) allow for increasing the electronic density of the material.

Once confirmed the metavalent character of MMBs in the octahedrally-coordinated phases of pnictogens and chalcogens, to finish this section, we want to remark that the multicenter character of the unconventional bond in the A_h and A_i phases of group-15 and -16 elements is consistent with previous calculations in PCMs characterized by the IpCOHP(2c) and the ICOBI(3c) values [39,40]. For that purpose, we have analyzed the values of the IpCOHP(2c) along the primary and secondary bonds of the A7 and A8 structures in pnictogens and chalcogens, respectively, at different pressures and also the ICOBI(3c) along the two bonds.

For example, As exhibits a decrease (increase) of IpCOHP(2c) along the primary d_1 (secondary d_2) bonds in As-I from -3.451 (-0.835) at 0 GPa to -3.135 (-2.733) at 35 GPa. This trend is indicative of the decrease (increase) of the strength of the primary (secondary) bond until they reach the same value once the As-II structure is attained. This pressure-induced "*trans influence*", i.e. influence of the secondary bond on the primary bond, is clearly evidenced for As in **Fig. 5a** by the *inverse* pressure dependence of the ES values of both primary and secondary bonds. On the other hand, the increase of the absolute value of ICOBI(3c) from -0.046 at 0 GPa to -0.076 at 35 GPa is clearly indicative of the increase of the multicenter (in this case three-center) interaction as one goes from As-I to As-II. According to Dronkowski and coworkers, the negative value of ICOBI(3c) indicates that these multicenter bonds are ERMBs [39]; however, we think that this interpretation of the value of ICOBI(3c) should be revisited as we will further discuss in section 4.

In any case, electron delocalization over more than two atoms in PCMs has been already proved theoretically [39] and is indeed proof of the *multicenter* character of the MMB. It can therefore be concluded that the unconventional MMB of PCMs and the A_h and A_i phases of group-15 and -16 elements is characterized by a blend of localized electrons between two atoms and delocalized electrons over more than two atoms. Electron delocalization is responsible for the sharing of *ca.* one electron (ES $\approx$ 1) between every two atoms in MMBs. The lower ES value in the MMBs than in covalent bonds indicates that the electronic charge shared between two atoms in MMBs is smaller than in covalent bonds. Consequently, MMBs are softer bonds than covalent bonds. The softness of MMBs has been experimentally demonstrated by the high probability of multiple events observed in laser-assisted field evaporation experiments of PCMs using atomic force microscopy [12,68,138], and confirmed by lattice dynamics studies [139]. Moreover, the transformation of the strong covalent *p*-type bonds into the softer MMBs in group-15 and -16 elements at HP, marked by the progressive softening of the covalent bonds as atomic coordination increases at HP, accounts for the softening of the optical phonon frequencies in their covalent *p*-type crystalline phases at low pressures, as already proved [52] and for the lower melting points of Bi and Po than of Sb and Te at RP and of Sb and Te than of As and Se, respectively [120].

As a summary of this section, we conclude that: i) Polonium is the only chalcogenide that shows fully symmetric MMBs at RP in either of the two known octahedrally-coordinated polymorphs and ii) group-15 (group-16) elements undergo a pressure-induced PT from the A7 (A8) phases, featuring a mixture of primary covalent *ppσ*-bonds and secondary bonds with LEPs at RP, to HP phases that show MMBs as the octahedral coordination is approached. Whereas the A_h phase is preferred for group-15 elements at HP, the A_i phase is preferred for group-16 elements at HP. In addition, we have shown that the change from the pre-MMB scenario to the MMB scenario is anticipated, for instance, by two measurable magnitudes: i) the change (from negative to positive pressure coefficient) in the optical phonon frequencies, i.e. sign change in Grüneisen parameters and ii) the increase of the average Born effective charge. The MMB scenario occurs at a smaller pressure along the series As-Sb-Bi and Se-Te-Po; a result consistent with the smaller structural distortion of Bi-I (Te-I) than Sb-I and As-I (Se-I) with respect to the A_h (A_i) phase. This result agrees with previous studies that relate the stronger structural distortion in different materials with larger *s-p* mixing and consequently with stronger LEP stereoactivity [29–33]. Consequently, our results are consistent with the equivalence of the effect of pressure and change of composition when going down the group to heavier elements in the periodic table [29–33], since pressure reduces the LEP stereoactivity in the same way as composition. Finally, we have concluded that the ES and ET values provided by the QTAIM theory not only confirm that bonds in the octahedrally-coordinated phases of pnictogens and chalcogens are MMBs but also can be used to trace in the 2D map the primary covalent bonds and the MMBs in the different crystalline phases of these elemental families and their changes with pressure and composition.

3. Mechanism of MMB formation in group-15 and -16 elements

Pressure allows fine-tuning of interatomic interactions by the gradual change of interatomic distances. This feature will allow us to delve deeper into the mechanism of the pressure-induced pre-MMB to MMB transformation in group-15 and -16 elements. For this purpose, we make use

of several theoretical bond descriptors, such as ES and ET, ρ and $\nabla^2\rho$, ELF, DOS, COOP, pCOHP, IpCOHP, and ICOBI that have been previously used to describe MMBs [12,34,39–44,57]. In particular, we analyze here the pressure dependence of the primary and secondary bond distances, d_1 and d_2, and their corresponding values of charge densities, ρ_{d1} and ρ_{d2}, and ELF, ELF_{d1} and ELF_{d2}, at the BCPs for the A7 (A8) phase of group-15 (16) elements. We also analyze the evolution of the pCOHP and COBI parameters and their integrated values along the two distances d_1 and d_2. These values will help us to understand the bonding, non-bonding, or antibonding character of the different orbitals involved in the different bonds [39–41,140–142]. Similar calculations will be also performed for the A_h and A_i phases of Po. Finally, we analyze the ELF isosurfaces [143] to see the evolution of the LEPs of the A7 (A8) phase of group-15 (-16) elements at HP, when they undergo the PT to the A_h (A_i) phase, and to understand the mechanism of the pre-MMB to MMB transformation.

First of all, we want to stress that the basics of the transformation from pre-MMB to MMB scenarios between three atoms (A, B, and C), either by the change in pressure or composition, was initially schematized by Lee and Elliott for GST [42–44] and proceeds according to the sequence from left to right displayed in **Fig. 7a-c**. **Fig. 7a** corresponds to the case of a B atom showing a strong primary covalent *pp*σ-bond with the A atom (both separated a short distance d_1) and a weak secondary bond with the C atom (both separated a large distance d_2) in which a LEP is involved. This case corresponds to $d_2/d_1 >> 1$ and we will show it is the typical case of As at RP. **Fig. 7b** corresponds to the case of a B atom showing a weakened primary covalent *pp*σ-bond with the A atom and a strengthened secondary bond with the C atom. We will show that this case corresponds to $d_2/d_1 > 1$ and is the typical case of Se and Te at RP and of As above 15 GPa. **Fig. 7c** corresponds to the case of a B atom showing a MMB with A and C atoms. Ideally, a fully symmetric, linear MMB, like those of the units plotted in **Fig. 3**, occurs when A and C atoms are exactly at the same distance from the B atom ($d_2/d_1 = 1$). This is the case of both phases of Polonium at RP, as already shown in the previous section.

Before analyzing the mechanism of MMB formation in group-15 and-16 elements, it must be noted that the scheme of **Fig. 7** also conforms to the progressive formation of hypervalent ERMBs in molecules already commented on by Hoffmann and coworkers [29,49,50,144,145] and recently reviewed [81]. It has been suggested that the formation of ERMBs occurs due to the existence of a mixture of primary bonds and secondary donor-acceptor bonds. These secondary bonds, apart from van der Waals interactions between LEPs of different atoms and other possible minor interactions, are considered to be caused by the interaction of the LEP (donor) of atom C in **Fig. 7a-b** and the antibonding orbital ($\sigma*$, acceptor) associated to the primary covalent *pp*σ-bond between A and B atoms in **Fig. 7a-b**. This means that secondary donor-acceptor bonding is due to the interaction of two antibonding orbitals since the LEP, with assumed nonbonding character, has in fact a certain antibonding character due to *s-p* mixing [29,33], as confirmed by pCOHP calculations later discussed concerning **Fig. 7d-f**. Many works have reported that the strength of the secondary bond is determined by the proper alignment of the directions of the LEP and σ*, which in turn depends on the d_2/d_1 ratio. In this way, the closer the A-B-C angle to 180° and the smaller the d_2/d_1 ratio the stronger the LEP-σ* interaction. This consideration suggests that, in general, the strength of the secondary bond is higher in stage 2 (**Fig. 7b**) than in stage 1 (**Fig. 7a**) due to the *trans influence* between primary and secondary

bonds. In the following, we will show that the pressure-induced transformation from the pre-MMB scenario to the MMB scenario proceeds via three stages (**Fig. 7a-c**) in group-15 elements and via two stages (**Fig. 7b-c**) in group-16 elements. The only exception is Po, which is already in stage 3 (**Fig. 7c**), as already mentioned.

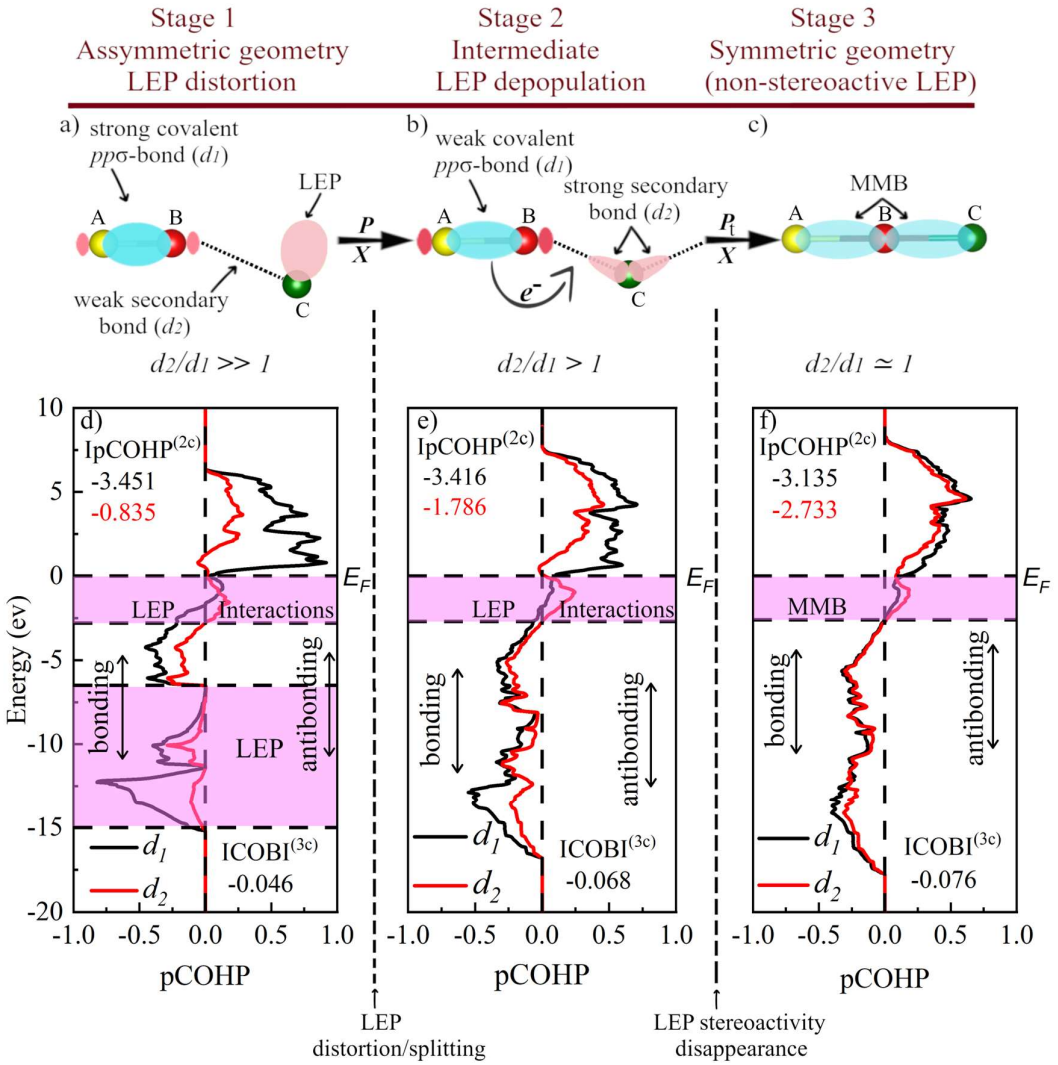

FIG. 7. Graphical representation of the mechanism of MMB formation under the effect of hydrostatic pressure, P, or change of chemical composition, X, by substituting atoms with their heavy analogs. a-b) Stages 1 and 2 correspond to classical primary covalent *ppσ*-bonds plus secondary bonds in group-15 (As, Sb, Bi) and group-16 (Se, Te) at RP, respectively. c) Stage 3 represents the MMBs present in α-Po and β-Po at RP as well as in the octahedrally-coordinated HP phases of As, Sb, Bi, Se, and Te. Blue isosurfaces correspond to the bonding orbital of the covalent A-B bond, as well as the MMB. Pink isosurfaces represent the antibonding orbital of the covalent A-B bond and the LEP of atom C. The color intensity of different interactions reflects the bond strength at the different stages. d-f) Projected crystal-orbital Hamilton populations (pCOHPs) for the As-I phase at 0, 20, and 35 GPa corresponding to the three stages, respectively. The colored regions in the pCOHP panels illustrate the LEP and its interactions. Vertical dashed lines indicate the limits of the LEP distortion and depopulation/delocalization stages.

It must be stressed that the above-described model of secondary LEP-σ* donor-acceptor interaction, which leads to the formation of hypervalent molecules, is a key concept of supramolecular chemistry that has been extensively revisited in the last two decades.

Traditionally, the LEP-$\sigma*$ interaction has been explained as a charge-transfer model in which part of the charge is transferred from the LEP donor to the $\sigma*$ acceptor. This *trans influence* is accompanied by an increase in the bond distance of the covalent bond. This interaction has been reinterpreted in the last decades in light of the σ-hole concept for secondary bonding [73,74,76–79,81]. According to the σ-hole bond model, the secondary donor-acceptor bond consists of an electrostatic interaction between an electrophilic (acceptor-like) moiety and a nucleophilic (donor-like) moiety. This Coulombic interaction is related to the more electropositive potential of the acceptor moiety (σ-hole) and the more electronegative potential of the donor moiety that are in turn related to their different electronic densities. In our work, the positive electrostatic potential (σ-hole) would be located at both ends of the primary covalent *pp*σ-bond (e.g. As—As) and would correspond to the antibonding orbital, while the negative electrostatic potential is located at the LEP. A key difference between the two models is that in the σ-hole bond model there is no net charge transfer from the donor to the acceptor, but a polarization or charge shift in the acceptor moiety, which is induced by the proximity of the donor moiety. The two models of charge-transfer and σ-hole for secondary bonding in group-15 and -16 elements will be further discussed in the next section once the mechanism of MMB formation in these families is clarified. Now let us see the mechanism of formation of MMBs in these two elemental families.

Group-15 elements. Experimental [94] and theoretical data show that the pressure-induced A7-to-A_h PT in As is characterized by the equalization of the three short primary intralayer, d_1, and the three large secondary interlayer, d_2, bond distances in As-I as pressure increases (**Fig. 8a**). Concomitantly, an equalizing trend is observed for ρ_{d1} and ρ_{d2} (**Fig. 8b**) and for ELF_{d1} and ELF_{d2} at BCPs (see **Fig. S12** in ESI). Remarkably, both ρ and ELF values for MMBs at P_t in As are smaller than those of covalent bonds at RP. Similar trends occur also in Sb and Bi during the A7-to-A_h PT and in Se and Te during the A8-to-A_i PT (see **Fig. S3, S5, S8, and S10** in ESI). Furthermore, similar trends have also been reported in IV-VI and V_2-VI_3 compounds [42,84,87,99]. Therefore, our results confirm that MMBs at P_t in group-15 and -16 elements are weaker than covalent bonds at RP, as already commented. In this context, it is worth noting that the covalent character previously attributed by many researchers to the MMBs in PCMs of the IV-VI family and Bi-III [52,137] is likely due to the relatively high values of ρ and ELF found in MMBs, despite they are typically somewhat smaller than for covalent bonds (ρ_{d1} and ELF_{d1}).

The most important point in **Fig. 8a-b** is that three distinct stages occur in As between 0 and 35 GPa. These three stages correspond to stages 1 to 3 in **Fig. 7a-c**. In stage 1 (up to 16 GPa), there is a weak (strong) decrease of d_1 (d_2) as well as a correspondingly small (large) increase of ρ_{d1} (ρ_{d2}). In stage 2 (from 16 to 25 GPa), there is a decrease of d_2 and an *anomalous* increase of d_1 as well as a corresponding decrease (increase) of ρ_{d1} (ρ_{d2}). Finally, once both primary and secondary bonds equalize (above 25 GPa) the A_h phase corresponding to stage 3 is reached. This stage is characterized by linear MMBs that show the *normal* decrease of the bond distance and increase of the bond charge density as pressure increases. A clearer picture of the three stages along the A7-to-A_h PT in As can be noted by the S-like behavior of d_1 vs. d_2 and ρ_{d1} vs. ρ_{d2} in As-I (see **Fig. 8c-d**), since d_2 (ρ_{d2}) always decreases (increases) with increasing pressure.

A clear distinction between stages 1 and 2 in As is provided by the sign change in the pressure coefficient of d_1 and ρ_{d1} around 16 GPa (**Fig. 8a-b**) due to the *anomalous* increase (decrease) of

d_1 (ρ_{d1}) that occurs in stage 2 above that pressure. These calculated *anomalous* trends agree with the results of previous calculations of the effect of pressure on As-I [102], and on As trimers [31], which left unnoticed. Unfortunately, the calculated increase of d_1 has still not been experimentally confirmed in pure As due to the limited resolution of the only published results based on a lab-based diffractometer [94] and the lack of more accurate results comming from synchrotron-based X-ray diffraction measurements. In any case, it must be pointed out that our results for As are also consistent with the increase of the short intrachain d_1 distance in Se at low pressures (see **Fig. S8a** in ESI) [146] and with the equalization of bonds at HP and the *anomalous* increase of the short bond distance at HP experimentally reported along the A7-to-A_h PT in elemental phosphorous [104].

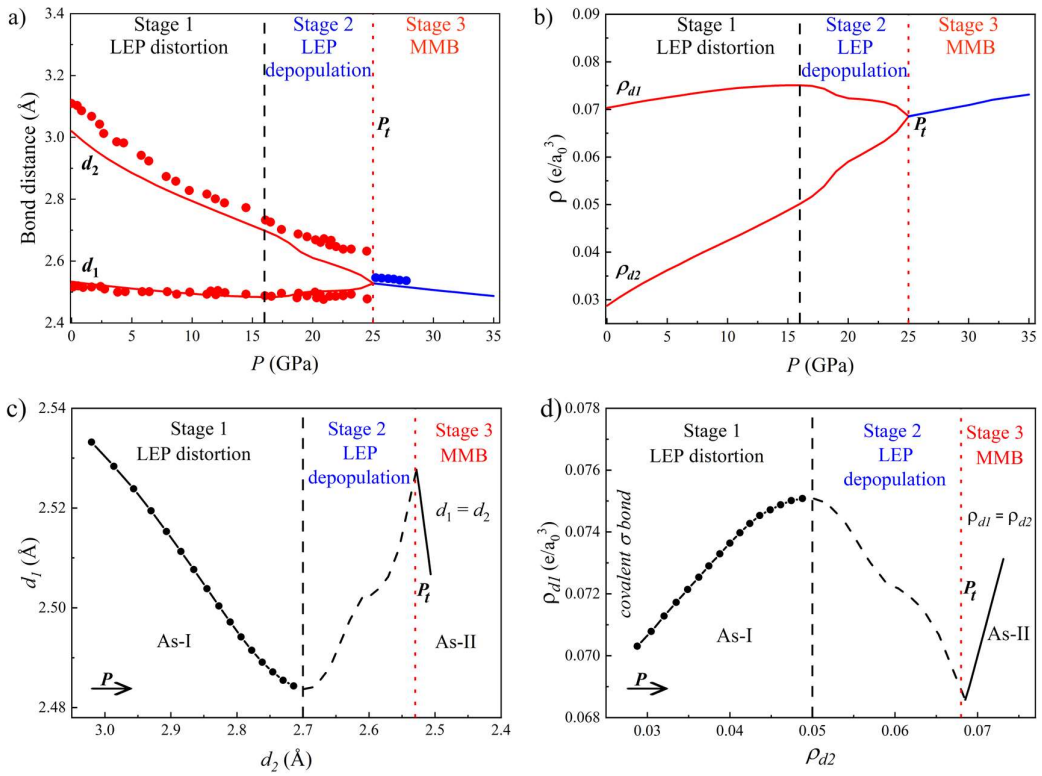

FIG. 8. Theoretical physical properties of As-I (A7, red) and As-II (sc, blue) as a function of pressure. a) Calculated (line) and experimental (circles) [95] first- and second-nearest neighbor distances first- and second-nearest neighbor distances, d_1 and d_2, respectively, in As-I and As-II crystals. b) Charge density at the BCP along the different bond distances, ρ_{d1} and ρ_{d2}, respectively, in As-I and As-II. c) Evolution of d_1 vs. d_2 for As-I. d) Evolution of ρ_{d1} vs. ρ_{d2} for As-I. Arrows in c) and d) indicate the direction of increasing pressure. *e* is the electron charge and a_0 is the Bohr radius. The three stages of the pre-MMB to MMB transformation are separated by vertical dashed and dotted lines.

Interestingly, the equalization of bond distances between primary covalent bonds and secondary weak close-shell interactions upon the increase of pressure or density was already commented in relation to the formation of multicenter bonds in molecules and an *anomalous* increase in the covalent bond distance was observed in the region close to the formation of the multicenter bond [31,51]. Moreover, simulations of the effect of pressure on elemental nitrogen have reported an *anomalous* increase of the intramolecular N—N bond distance at HP [92].

Simulating the evolution at HP of the trimer $(N_2)_3$ system, where there is a coexistence of triple intramolecular N—N bonds in N_2 and secondary intermolecular N_2 interactions at RP, it was found that the triple bond is destroyed at HP and single N—N bonds are formed [90]. An equalization of intramolecular and intermolecular N—N distances in this system occurs at HP, together with an *anomalous* increase of the intramolecular N—N bond distance until both distances reach similar values at HP. Similarly, an equalization of intramolecular and intermolecular H—H distances occurs in elemental hydrogen at HP together with an *anomalous* increase of the intramolecular bond distance above 100 GPa [147–150]. Simulating the ring $(H_2)_3$ system, the equalization of distances in hydrogen has been understood as due to the progressive charge transfer from intramolecular H—H bonds to intermolecular H—H bonds due to the *trans influence* between the primary and the secondary bonds [150]. The pressure-induced *trans influence* and the corresponding *anomalous* increase of the bond distance of original covalent bonds in group-15 and -16 elements as well as in nitrogen and hydrogen will be further discussed in section 4 concerning the MMB nature.

For many years, the *trans influence* in the A7 structure of pnictogens was supposed to exist and invoked to explain the decrease of the frequencies of the optical phonons as well as the increase in the acoustic phonon frequencies and, consequently, the increase of the elastic constants at HP [108,109]. The inverse behavior of ρ_{d1} and ρ_{d2} in As at stage 2 (above 16 GPa) can also be understood by the *trans influence* that results in a charge transfer from the primary covalent bond to the secondary bond as pressure increases until they reach the same value at Pt (once the MMBs are formed). This charge transfer is clearly shown by the evolution of ES of both primary and secondary bonds in As as pressure increases (**Fig. 5a**), as already mentioned.

As regards stage 3 in As (As-II), the *normal* decrease (increase) of the interatomic bond distance (bond charge density) of MMBs in this stage are common behaviors of covalent materials with sp^3 geometry and no secondary bonding, such as zinc-blende Si and Ge [151]. This *normal* behavior of the bond distances and the charge densities of MMBs is consistent with the experimentally and theoretically observed hardening of all phonons in As-II (**Fig. 2a**), as it occurs for Si and Ge [105,152]. This *normal* behavior in As-II contrasts with the soft optical phonons of the A7 phase in As and of the *R*3*m* phase in GeTe[13]; i.e. in the pre-MMB scenario. The *normal* behavior in *sc*-As and in zinc-blende Si and Ge is the result of the lack of *trans influence* due to the lack of secondary bonds in these crystalline structures; in other words, there is only a single type of bond in these crystalline structures. Therefore, we tentatively conclude that the soft optical phonons in materials with primary covalent *pp*σ-bonds and secondary bonds, as confirmed by a recent three-center interaction model [52], are a clear fingerprint for the previously suggested instability of these primary bonds at HP [153–156]. The softening of optical phonons in *p*-type covalent materials can be understood as an instability of the structure due to the transformation of covalent bonds into MMBs at HP. This instability of covalent *p*-type materials is analogous to the instability of tetrahedrally-coordinated sp^3 ionocovalent materials, such as zinc-blende Si and Ge, whose soft acoustic modes at the Brillouin zone edges are signatures of the instability of the sp^3 σ-bonds against octahedral coordination at HP [157].

A deeper understanding of chemical bonding in As can be obtained from the reciprocal-space (band) picture [158,159], since the three stages of As can be distinctively characterized by

orbital-based methods. The electronic bands and DOS of As-I at 0 GPa have been thoroughly discussed in the literature and are briefly commented on in section 6 of the ESI. Here we analyze the pCOHP (**Fig. 6d-f**) and COBI (**Fig. S13** in ESI) as well as their integrated values (IpCOHP, ICOBI(2c), and ICOBI(3c)) along the d_1 and d_2 bonds in As-I at 0, 20, and 35 GPa that correspond to stages 1, 2, and 3, respectively. The most important point is that bands with antibonding character (positive value of pCOHP [140]) appear below the Fermi level both along d_1 and d_2 at RP, as well as in Te-I [142]. These bands come from the interaction between the LEP and the bonding orbital of the covalent bond (along d_1) and between the LEP and the antibonding orbital of the covalent bond (along d_2), as already discussed by Hoffmann and coworkers [49]. The antibonding character of these bands, in which LEPs are involved, comes from the *s*-*p* mixing, i.e., the mixing of the *s*-type electrons of the LEP and the *p*-type electrons of the bonding and antibonding orbitals of the covalent bond [29,33].

In stage 1 of As-I at 0 GPa (**Fig. 7d**), the larger pCOHP absolute values of the bonding bands (negative values of pCOHP [140]) as well as the larger IpCOHP and ICOBI(2c) values along d_1 than along d_2 indicate a much stronger bonding in primary than in secondary bonds, as already commented at the end of section 2. In addition, since negative (positive) values of ICOBI(3c) are interpreted to correspond to electron-rich or 3c-4e (electron-deficient or 3c-2e) interactions [39,40], the small, negative ICOBI(3c) value compared to the high ICOBI(2c) value along d_1 seems to indicate that electron-rich three-center interactions are small in As-I at 0 GPa. In stage 2 of As-I at 20 GPa (**Fig. 7e**), the profiles of the pCOHP along d_1 and d_2 become more similar (both above and below the Fermi level). The decrease (increase) of the strength of primary (secondary) interactions due to the *trans influence* is reflected in the smaller (larger) values of the pCOHP than at 0 GPa. Moreover, the antibonding bands below the Fermi level along d_1 (d_2) show a smaller (larger) value of the pCOHP in comparison to As-I at 0 GPa. This can be interpreted as if the LEP in this stage experiences a much larger interlayer interaction (LEP-σ^*) than intralayer interaction. We interpret this feature as the signature that the LEP starts to become inactive (non-stereoactive) with increasing pressure. The smaller and weaker (larger and stronger) primary (secondary) bonds in stage 2 than in stage 1 due to *trans influence* are also reflected in the smaller (larger) values of IpCOHP(2c) and ICOBI(2c) along d_1 (d_2) [39,40]. Moreover, the ICOBI(3c) value at 20 GPa shows a much larger negative value than at 0 GPa which seems to be consistent with the process of multicenter bond formation in As at HP. Finally, pCOHP profiles are similar for the primary and secondary bonds in As-I at 35 GPa (**Fig. 7f**) as expected for MMBs in stage 3. The slightly different profiles for both bonds are due to the slight distortion of the cubic symmetry in As-I with respect to As-II at 35 GPa, as already mentioned (both pCOHP profiles are exactly equal in As-II at 35 GPa, see **Figure S13d** in ESI).

At this point, we want to stress that our pCOHP results for As between stages 1 and 3 are consistent with those previously reported for Te, where completely different pCOHP profiles for the two different bonds in Te-I contrast with the similar profiles of the two different bonds in Te-II [142]. The similarity of the bonding orbitals along d_1 and d_2 in stage 3 of As (also in Te-II in Ref. [142]) indicates that *p*-type orbitals contribute equally to all bonds since they are of similar length, while *s* electrons forming part of the LEP are inactive in As-II and very weakly active in Te-II (since there is a small distortion of the triclinic structure of Te-II with respect to the cubic A_h structure that is similar to that of the HP A_i phase of Te that we have calculated). This result

is consistent with the non-layered 3D structure of As-II and Te-II (and the other phases of As and Te at higher pressures). The most representative feature of stage 3 in As (As-II) is that an intense, broad antibonding band appears in the pCOHP just below the Fermi level. Unlike in the pre-MMB scenario, this band overlaps with the antibonding orbitals of the conduction band, so the value (negative) of the pCOHP at the Fermi level is different from zero. This result is the same as previously obtained for Te-II and the antibonding character at the Fermi energy in As-II (Te-II) is clearly due to the repulsion between the inactive (weakly active) LEPs at reduced interlayer (interchain) distances [142]. Noteworthy, the loss of the LEP stereoactivity and the occurrence of a flat/steep band near the Fermi level has been postulated as a signature for superconductivity in the HP phases of group-15 and -16 elements [142], and also for the transition between trivial- and topological-insulating phases in the same materials [160]. In addition, the absolute value of ICOBI(3c) for As–As–As interaction in As gradually increases (in negative value) over the three stages (**Fig. 7d-f**). The ICOBI(3c) value at stage 3 in As-II is similar to that recently reported for β-GeTe, in which ERMB formation was suggested [39].

Regarding Sb and Bi, our simulations also confirm the presence of the three stages of the mechanism of MMB formation along the A7-to-A_h PT (**Fig. S3, S5, and S12b-c** in ESI). In particular, Sb-I is in stage 1 at 0 GPa and in stage 2 above 3.5 GPa, whereas stage 3 should occur experimentally in Sb-II above 8 GPa. On the other hand, Bi-I is in stage 1 (close to stage 2) at 0 GPa and in stage 2 (close to stage 3) in Bi-II at 2.5 GPa. Since the A_h phase has not been experimentally reported in Bi, stage 3 should occur experimentally in Bi-III above 2.7 GPa, as already pointed out in the previous section. Interestingly, our results obtained for Bi are consistent with the comments of Häussermann et al. [137], who stated that the electronic band structure of Bi-III shows a Fermi level located in a valley in the bands formed by bonding and antibonding p-orbitals with a "*significant covalent bonding contribution"*. They also noted that the "*covalent bonding contribution*" in Bi-III is no longer present in the A2 phase of group-15 elements that occurs at higher pressures, where a full electron delocalization is found, as expected in metallic bonding. In this context, we consider that the term "*significant covalent bonding contribution"* should be now understood as the MMB contribution in Bi-III because MMBs are also directional, like covalent bonds, and unlike metallic bonds. Finally, we have to stress that a progressive decrease of the pressure range of stages 1 and 2 is observed on going from As (stage 1: 0 - 15 GPa; stage 2: 15 - 25 GPa) to Sb (stage 1: 0 - 3.5 GPa; stage 2: 3.5 - 7 GPa) and Bi (stage 1: 0 - 2.5 GPa; stage 2: 2.5 - 2.7 GPa).

Group-16 elements. Experimental and theoretical data show that the pressure-induced A8-to-A_i PT in Se and Te is characterized by the equalization of the two short primary intrachain (d_1) and the four large secondary interchain (d_2) bond distances as pressure increases (**Fig. S8a and S10a** in ESI). Concomitantly, an equalizing trend is observed for ρ_{d1} and ρ_{d2} (**Fig. S8b and S10b**) and for ELF_{d1} and ELF_{d2} at BCPs (**Fig. S12d-e** in ESI). The most important point is that two stages occur in Se and Te at HP in the above-mentioned figures that correspond to stages 2 and 3 in **Fig. 7b-c**. In stage 2 (near RP), there is a strong decrease of d_2 and an *anomalous* increase of d_1 that matches with available experimental values for Se (see **Fig. S8a**) [146]. This *anomalous* increase of d_1 is similar to that previously commented of As in stage 2 above 16 GPa. Correspondingly, there is an increase (decrease) of ρ_{d2} (ρ_{d1}) in Se and Te, respectively. Finally, in stage 3, the A_i phase is reached and both primary and secondary bonds of Se and Te become

MMBs that show a *normal* decrease (increase) of the bond distance (bond charge density) at HP. Again, the partial S-like behavior of d_1 vs. d_2 (**Fig. S8c and S10c**) and ρ_{d1} vs. ρ_{d2} (**Fig. S8d and S10d**) provides a clearer picture of the two stages present in Se and Te at HP.

Regarding the two mentioned stages of the pre-MMB to MMB transformation in Se and Te, it is worth noting that the behavior of bond distances and bond charge densities in stage 2 of Se and Te is similar to that previously found in stage 2 in pnictogens. The inverse behavior of ρ_{d2} and ρ_{d1} in elemental chalcogens at HP is caused by the *trans influence* between primary and secondary bonds (see ES in Se **Fig. 5b**), as already mentioned for pnictogens in stage 2. As for pnictogens, the *trans influence* was invoked a long time ago in elemental chalcogens to explain the strong softening of the A_1 mode of the A8 phase as well as the increase of the frequencies of the acoustic phonons and the values of the elastic constants in Se-I and Te-I at HP [153,161,162]. On the other hand, the *normal* decrease of the interatomic bond distance and the increase of the bond charge density of MMBs in stage 3 are consistent with the hardening of all phonons in the distorted A_i phase (**Fig. S7d and S9d**). Again, it is interesting to remark that the pressure range of stage 2 decreases in group-16 elements from Se (0 - 23 GPa) to Te (0 - 7 GPa); i.e., it decreases for heavier cations, as already observed for group-15 elements.

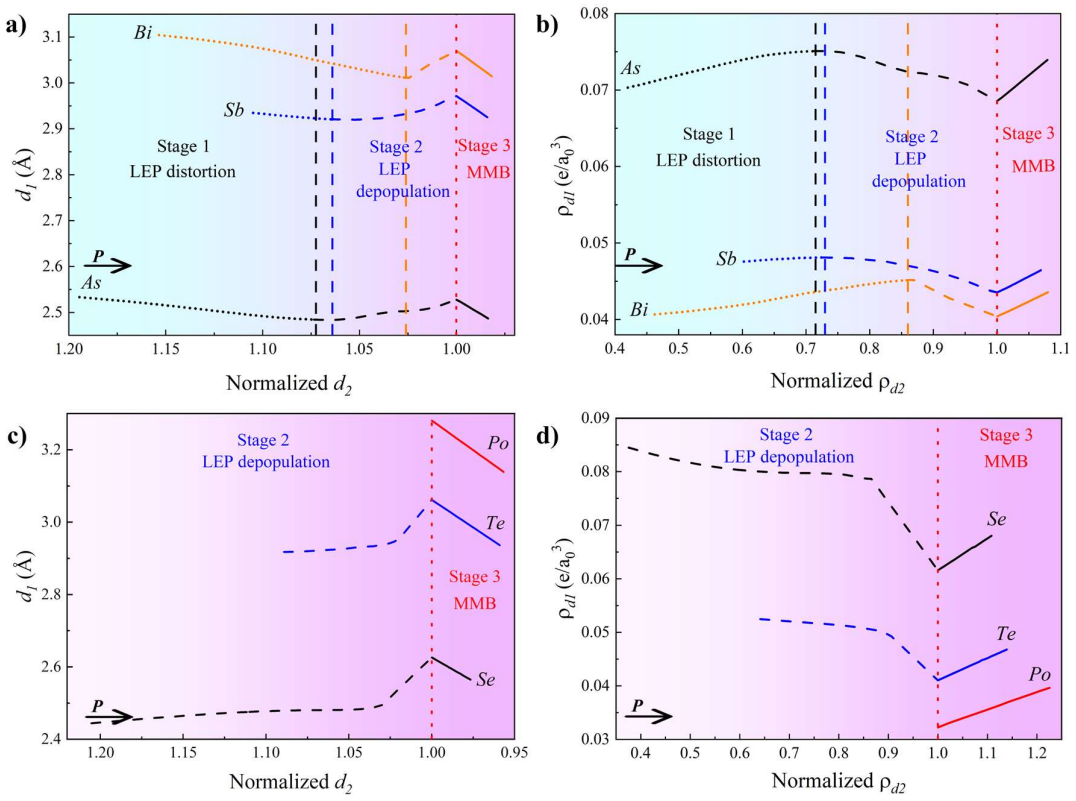

FIG. 9. Calculated primary bond distance, d_1, vs. the normalized secondary bond distance, d_2, in group-15 (a) and -16 (c) elements. Calculated charge density at BCP of the primary bond, ρ_{d1}, vs. the normalized charge density for the secondary bond, ρ_{d2}, in group-15 (b) and -16 (d) elements, where *e* is the electron charge and a_0 is the Bohr radius. Normalization is performed with respect to the values at P_t. The stages for each group of elements are separated by vertical dashed and dotted lines. The gradual change in the background color reflects the strength of the secondary bonds until the MMB is formed at the normalized value of 1.

A completely different behavior from pnictogens and chalcogens is found in both phases of Po. The *normal*, slight decrease (increase) of the bond distance (charge density) in both phases of Po at HP (**Fig. 4a**) clearly evidence that both phases of Po do not show several stages at HP. The reason is that they are already in stage 3 at RP because they show fully symmetric MMBs at RP. The pCOHP features of α-Po and β-Po at RP (**Fig. S11d**) are very similar and show similar values of IpCOHP(2c) as those found in As-II (**Fig. S13d**). Again, the negative value of ICOBI(3c) suggests the presence of ERMBs according to Dronkowski and coworkers [39,40]. In this context, we must stress that, although the value of ICOBI(3c) in Po is smaller than in As-II, the ratio ICOBI(3c)/IpCOHP(2c) is larger in Po than in As-II. This picture is also consistent with the pressure dependence of the ES (**Fig. 5c**) and ELF (**Fig. S12f**). Note that the ES≈ 1 for both phases of Po and there is a negligible increase with pressure. This is an expected result for the MMBs in stage 3 since there is no *trans influence* in this stage and bonds show no gain or loss of charge at HP, just a monotonous decrease (increase) of bond distance (charge density).

A clearer comparison among all the studied pnictogens and chalcogens regarding the mechanism of MMB formation can be seen by plotting d_1 and ρ_{d1} vs. normalized d_2 and normalized ρ_{d2}, respectively (**Fig. 9**). This figure nicely shows the three (two) stages of the MMB formation mechanism in group-15 (16) elements. Moreover, the strength of the secondary interaction along the three stages can be traced by the change in the background ground (from light blue to pink). The comparison of all elements in normalized values allows us to observe the relative decrease of the pressure range of both stages 1 and 2 in pnictogens and of stage 2 in chalcogens upon moving down the group (from As to Bi and from Se to Po), with the only exception of Bi due to the problems with the PBEsol calculations at HP previously mentioned. This outcome confirms our earlier observations of the pressure ranges of these stages in elemental pnictogens and chalcogens. Therefore, we conclude that the pressure-induced transformation from the pre-MMB scenario to the MMB scenario in group-15 (16) elements proceeds via three (two) stages, being Po the only element of these two families whose two crystalline structures feature MMBs at RP.

At this point, we want to stress that several questions regarding the mechanism of MMB formation are still not clearly understood and need further exploration: Why pnictogens show a three-stage mechanism and chalcogens only a two-stage one? Why the A_h phase is preferred by pnictogens at HP, while the A_i phase is preferred by chalcogens at HP? What is the relation between stage 2 in group-15 and -16 elements?

A deeper understanding of the MMB formation mechanism can be obtained if the reciprocal-space (band) picture is complemented by the real-space (bond) picture [143]. In particular, the analysis of the ELF topology is a good tool for understanding the formation of secondary bonds, as already shown for CO_2 [163]. Therefore, we have analyzed the ELF isosurfaces corresponding to the values of the secondary bonds in which LEPs for the studied elements at different pressures are involved (**Fig. 10**). In group-15 elements, each atom in the layered A7 structure at RP (stage 1) is characterized by a single ELF attractor perpendicular to the layers corresponding to the LEP (**Fig. 10a**). This single-basin LEP is formed by *s*-type orbitals, and it is not aligned along any of the three secondary bonds of the A7 structure. At a certain pressure, the *s*-type LEP dissociates or splits into three similar lobes (onset of stage 2) that properly align with the

directions of the three secondary bonds (**Fig. 10b**). At Pt (upon the A7-to-A_h PT), the new three lobes along the secondary bonds become equal to the primary bonds, which marks the onset of stage 3. At this stage, six lobes appear around each atom corresponding to the three pairs of MMBs in the A_h phase (**Fig. 10c**). It is important to mention that six equal ELF lobes are also present in α-Po at RP. Moreover, six ELF attractors of similar size to those of the A_h phase in As are also observed in Bi-II (**Fig. S6f**), thus confirming that Bi-II already exhibits asymmetric MMBs. Therefore, we conclude that six equal ELF attractors are characteristic of fully symmetric MMBs in the hypercoordinated multicenter unit with cubic symmetry shown in **Fig. 3c**.

Considering the LEP picture, the results in **Fig. 10a-c** for pnictogens can be understood in the following way: In stage 1, the single-basin LEP found at RP suffers a considerable distortion due to the increasing interlayer interaction as pressure increases that is caused by the strong compression of the interlayer distance. At the same time, the *trans influence* in stage 1 slightly increases the charge of the secondary bond at the expense of the primary covalent *ppσ*-bond. The LEP distortion ends with the splitting of the single ELF basin into three ELF basins (onset of stage 2) that are aligned along the three secondary bonds. On further increase of pressure, the LEP starts to become inactive due to a gradual decrease in the LEP charge. This is evidenced in As by the decrease of the strength of the band located below the Fermi level in the pCOHP profile along the primary bond (**Fig. 7d-f**). In other words, the LEP becomes depopulated in stage 2 as pressure increases. This result is consistent because the decrease of the LEP stereoactivity at HP is a well-known phenomenon in materials [164]. In other words, the LEP becomes depopulated in stage 2 as pressure increases. This result is consistent with the LEP depopulation (or delocalization) process already reported in Te at HP [160]. Concomitantly, a much larger *trans influence* occurs in stage 2 than in stage 1 (**Fig. 5a**), which is consistent with the strong decrease of phonon frequencies in As and Sb above 16 and 4 GPa, respectively. The *trans influence* ends at P_t when the secondary bonds acquire equal or almost equal charge to the primary bonds (onset of stage 3), so six lobes or basins are observed around each atom corresponding to the three pairs of orthogonal MMBs in the A_h phase.

A similar lecture on the ELF isosurfaces can be done for chalcogens. Each Se and Te atom in the A8 structure at RP (stage 2) is characterized by two ELF attractors or lobes that are already aligned in the directions of two of the four secondary bonds, i.e. they form an angle of nearly 180° with the nearest covalent bond (**Fig. 10d**). These features agree with previous calculations [142,160], and are typical of *p*-type LEPs. In other words, there is a *p*-type LEP distributed along two (of the four) secondary bonds of each atom of Se and Te at RP and no LEP lobe pointing along the other two secondary bonds of the same atom. As pressure increases, the two LEP lobes become distorted so that they spread over the four secondary bonds. Finally, upon the A8-to-A_i PT at P_t (stage 3), an ELF attractor with a toroidal shape is observed around each atom (**Fig. 10e**). This toroidal shape of the ELF is also found in β-Po at RP. Therefore, we conclude that a toroidal ELF attractor is characteristic of MMBs in the hypercoordinated multicenter unit with rhombohedral symmetry shown in **Fig. 3c**.

The results in **Fig. 10d-e** for chalcogens can be understood in the following way: In stage 2, the *p*-type LEP of Se and Te at RP shows two ELF basins aligned along two of the four secondary bonds. This stage of chalcogens mirrors stage 2 of pnictogen, where the lobes are also properly

aligned along the secondary bonds. Therefore, it seems that group-15 and -16 elements show a different number of stages that are related to the different LEP distribution (or kind of LEP) involved in the secondary bonds. Moreover, the relation between stage 2 in both pnictogens and chalcogens is now clear and it can be understood why the short primary bond distance (charge density) shows an *anomalous* increase (decrease) with increasing pressure in both cases at this stage. The reason is the strong *trans influence* present in this stage of the pre-MMB to MMB transformation that is also responsible for the strong decrease of the A_1 phonon frequencies in Se and Te already at RP. All the above results are consistent with previous results for Te at HP [142,160]. Finally, the *trans influence* ends at P_t when the secondary bonds acquire equal or almost equal charge as the primary bonds (onset of stage 3).

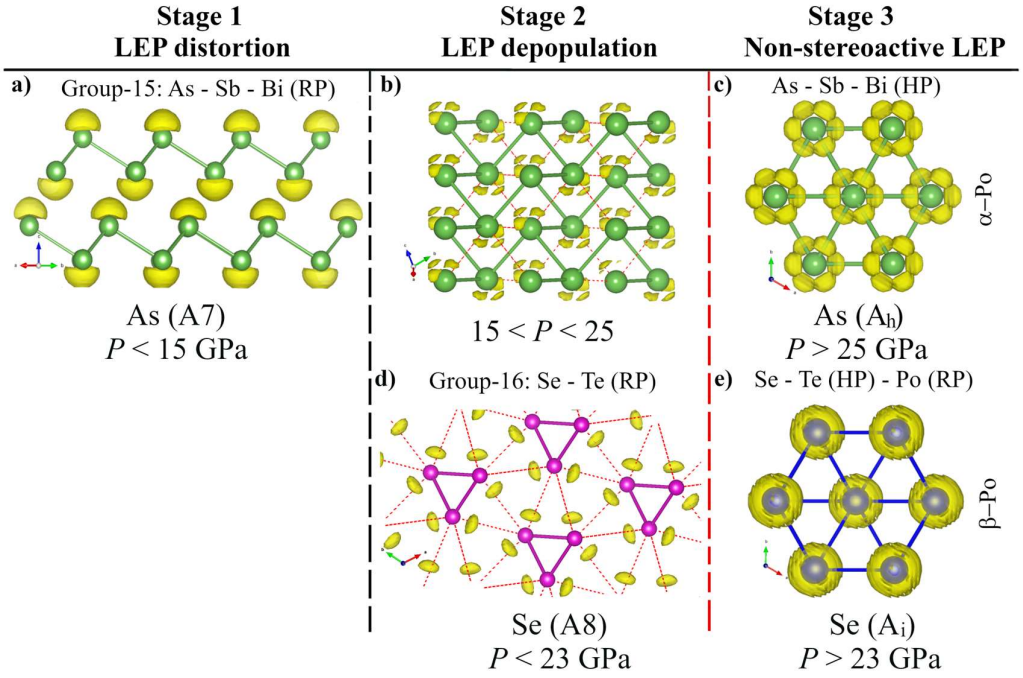

FIG. 10. ELF isosurfaces of elemental pnictogens (a-c) and chalcogens (d-e) at the three possible stages of the mechanism of MMB formation at different pressures. RP and HP stand for room and high pressure, respectively. The LEP basins are defined by an ELF isosurface (yellow color) arbitrary choice for element/stage. At RP, As, Sb, and Bi are located in stage 1, Se and Te are located in stage 2, and Po is located in stage 3.

As previously mentioned for pnictogens, the *p*-type LEP of chalcogens in stage 2 becomes gradually inactive as pressure increases due to the LEP depopulation/delocalization; however, the behavior of the LEP of chalcogens at this stage is different from that of pnictogens. In stage 2 of chalcogens, the ELF basins of the *p*-type LEPs become increasingly distorted with increasing pressure and become elongated towards the direction of the two secondary bonds with no ELF attractor at RP. This behavior is consistent with the electron transfer of the *p*-type LEP to the antibonding orbitals in Te-I at HP reported in Ref. [160] and also with the breakdown and delocalization of the LEP in Te-I at HP, so that these electrons become itinerant in Te-II as suggested in Ref. [142]. These results contrast with *s*-type LEPs in group-15 elements that barely change their profiles in stage 2 as they become progressively inactive. Due to the itinerant electrons, the ELF isosurface of Se and Te at the end of stage 2 shows a toroidal shape around each atom that is maintained in stage 3 and is characteristic of the A_i phase and different from

that of the A_h phase, where no itinerant electrons are observed. These itinerant electrons in the A_i phase can be ascribed to the extra valence electron present in group-16 elements as compared to group-15 elements. Therefore, it is clear why group-15 elements with five valence electrons tend to the A_h phase at HP, as rationalized by Papoian and Hoffmann [51], and why group-16 elements with six valence electrons tend to the A_i phase at HP.

Now we are in a better position to show the correlation between the three (two) stages found in group-15 (16) elements with the three stages represented in **Fig. 7a-c** and and their extension to IV-VI and V_2-VI_3 compounds related to PCMs. Stage 1 in **Fig. 7a** corresponds to a material with primary, short, and strong covalent 2c-2e *pp*σ-bonds (distance d_1) between A and B atoms and secondary, large, and weak bonds to atom C (distance d_2), which usually corresponds to a ratio $d_2/d_1 \gg 1$. This stage occurs in materials showing single-basin-type LEPs, such as pnictogens at RP, and it could be also the case for isoelectronic IV-VI compounds showing no *rs* structure at RP (GeS, GeSe, α-GeTe, SnS, and SnSe) as well as V_2-VI_3 compounds showing no tetradymite-like structure at RP (As_2S_3, As_2Se_3, α-As_2Te_3, Sb_2S_3, Sb_2Se_3, and Bi_2S_3). The step going from stage 1 to stage 2 is characterized by the single-basin-type LEP dissociation or splitting, i.e. the LEP in stage 1 splits into several basins aligned along the directions of the secondary bonds. Therefore, stage 2 (**Fig. 7b**) corresponds to a material with weakened primary covalent *pp*σ-bonds and strengthened secondary bonds caused by the charge transfer (*trans influence*) from the primary bonds to the secondary bonds. This stage occurs upon the decrease of the d_2/d_1 ratio ($d_2/d_1 > 1$) caused by either the effect of pressure or composition. Stage 2 is the step before the formation of the MMB and asymmetric MMBs are likely formed in stage 2 for values of d_2/d_1 close to 1 (tentatively below 1.05 - 1.10). Stage 2 is observed in materials with *p*-type LEPs at RP, such as Se and Te, and also in materials with single-basin-type LEPs at HP, such as pnictogens and perhaps the above commented IV-VI and V_2-VI_3 materials. The step going from stage 2 to stage 3 is characterized by the disappearance (or almost) of the LEP stereoactivity, which finally leads to octahedral coordination in materials with *p*-type bonds. Curiously, the decrease of the LEP stereoactivity in group-15 and -16 elements at HP on approaching the octahedral coordination is related to the appearance of superconductivity in all these elements at HP, except for Bi, which already shows superconductivity at RP [142,165,166]. Finally, stage 3 (**Fig. 7c**) ideally corresponds to a material with fully developed and symmetric MMBs and with equal A–B and B–C bonds that have one of the hypercoordinated multicenter geometries represented in **Fig. 3**. This stage occurs for $d_2/d_1 \approx 1$. For instance, stage 3 occurs in the A_h and A_i phases of Po at RP and in octahedrally-coordinate pnictogens and chalcogens at HP. This stage with MMBs is also observed at RP in the *rs* phase of IV-VI PCMs and of related ternary compounds, such as $GeSb_2Te_4$ and GST. Moreover, stage 3 can be considered to be also present at RP in the tetradymite-like phases of V_2-VI_3 PCMs (Bi_2Se_3, β-As_2Te_3, Sb_2Te_3, and Bi_2Te_3) [69] and of ternary IV-V_2-VI_4 compounds ($GeSb_2Te_4$, $SnSb_2Te_4$) [99], although not all atoms in the tetradymite-like phase show MMBs due to the layered nature of the tetradymite-like phases. The above observations support the idea already mentioned that the LEP stereoactivity decreases at HP and on going down a group in the periodic table. A total disappearance of the LEP stereoactivity is noticed in stage 3 if a cubic phase is obtained, such as in the A_h structure (of P, As, and α-Po) or the *rs* structure (of IV-VI PCMs). However, a residual LEP stereoactivity is observed in stage 3 if a distorted cubic phase is obtained, such as the distorted *sc* phases (of Bi-II and Bi-III) and the rhombohedral phases (of group-16 elements and tetradymite-like V_2-VI_3 PCMs).

The unanswered question regarding LEP stereoactivity, already posed by Papoian and Hoffmann more than 20 years ago [51], is why α-Po crystallizes in the A_h phase at RP and low temperatures if chalcogens have an extra electron that tends to distort the *sc* structure typical of pnictogens with five valence electrons. This distortion leads chalcogens to crystallize in the rhombohedral A_i phase of β-Po at HP. Papoian and Hoffmann suggested that the sixth electron of α-Po could be divided over the three *p*-bands (1/3 to each p_x, p_y, and p_z); therefore, the extra electron in chalcogen atoms would be shared with the neighbors. However, our results show that the extra electron is not shared between the chalcogen atoms in the MMBs since the values of electrons shared between two atoms are similar in both phases of Po (**Fig. 5c**) and even slightly smaller than those of the A_h phase of As-II (**Fig. 5a**). Instead, our results suggest that the extra electron in α-Po is resonating between the six lobes of the ELF of the A_h phase since the values of the ELF isosurfaces showing the inactive LEP in the A_h phase are smaller in As-II (0.825) than in α-Po (0.875). In other words, there is a larger charge density at the inactive LEP in α-Po than in As-II. Therefore, it looks like that low temperature helps to freeze the extra *p*-type electron of Po into the lobes of the inactive LEP. It remains to be seen if this effect also occurs in Se and Te at HP and low temperatures or if it is only possible in Po due to the secondary periodicity caused by the strong spin-orbit interaction (relativistic effect) [167].

Before finishing this section, it must be commented that our observation of three (two) stages in group-15 (16) elements, which is characterized by the progressive equalization of primary and secondary bonds at HP and includes the *anomalous* increase of bond distances of covalent bonds, is consistent with the experimental observation of bond equalization and *anomalous* elongation of short covalent bonds in trimers during the process of ERMB formation. These features were observed in molecules forming trimers of Sb and Te with halogen atoms by Hoffmann and coworkers, and later reploted by Lubchenko and coworkers [31,50]. They attributed the *anomalous* increase of the short covalent bond to *trans influence* corresponding to stage 2, despite that no critical bond distance was noted by those authors. Support for the existence of the proposed stages has been recently provided by the existence of critical points marking regions separating the continuum between supramolecular bondings and covalent bonds [80].

Noteworthy, we consider that the three stages for group-15 elements show a parallelism with the molecular, semimolecular, and atomic/polymeric stages that have been evidenced but not fully explained in nitrogen and hydrogen at HP [88,147–150]. As previously remarked, the pressure dependence of the intramolecular and intermolecular bond distances in N_2 and H_2 seems to show different stages between the pure covalent molecular stage and the HP metallic atomic stage. A deep analysis of these systems would require future calculations that are out of the scope of the present paper. In any case, the three-stage mechanism we propose for pnictogens seems to be consistent with the simulations of the $(N_2)_3$ system at HP carried out by Hoffmann and coworkers [88]. They pointed out that there is a significant contraction of the intermolecular distance (contraction of van der Waals region between N_2 molecules) and a corresponding negligible change of the intramolecular distance at low pressures (molecular regime, stage 1). This stage is followed by a pressure region in which there is an *anomalous* increase of the intramolecular distance once the intermolecular distance decreases below 1.6 Å (semimolecular regime, stage 2). Finally, a third pressure region was found where there is a

normal contraction of both intramolecular and intermolecular bond distances once all single N—N bonds are formed (atomic/polymeric regime, stage 3). Interestingly, a similar behavior has been observed in hydrogen at HP [147–150]. A *normal* decrease of both intramolecular and intermolecular H—H distances up to 100 GPa (stage 1) is followed by an *anomalous* increase (decrease) of the intramolecular (intermolecular) as pressure increases (stage 2), caused by the charge transfer from intramolecular to intermolecular bonds [147–150]. The *trans influence* ends once both bond distances equalize and each bond has a single electron per atom pair, i.e., all H—H bonds are 2c-1e bonds (stage 3). This seems to be the case above 500 GPa once the atomic phases of hydrogen appear [147–150].

As a summary of this section, we conclude that we have evidenced, by using the bond and band pictures, that the transformation from the pre-MMB scenario at RP to the MMB scenario in group-15 and -16 elements at HP proceeds by gradually increasing the electronic density. This result agrees with the view of Lubchenko and coworkers [31,89], but disagrees with the sudden change of coordination and properties between materials with covalent bonds and MMBs previously suggested by Wuttig and coworkers upon change in composition between PCMs and non-PCMs of the IV-VI and V_2-VI_3 families [69]. Unlike what was previously assumed, we have shown that the transformation process involves several intermediate stages until fully (or almost fully) symmetrical MMBs are formed. In particular, we have evidenced that there is a mechanism of MMB formation that comprises three stages (two stages) in group-15 (16) elements. The mechanism seems to be governed by the kind of LEP involved in the secondary interaction. Therefore, we conclude that the LEP stereoactivity, related to the *s*-*p* mixing, is the primary factor that rules the MMB formation in group-15 and -16 elements and by extension in binary IV-VI and V_2-VI_3 chalcogenides and other related complex chalcogenides. This result agrees with previous works that reflect the importance of *s*-*p* mixing in these elemental families [29–33]. We consider that this universal mechanism is expected to apply to most materials evolving from the pre-MMB scenario (with primary covalent *ppσ*-bond plus a secondary interaction with the participation of LEPs) to the MMB scenario either due to compression or to change of composition by heavier elements. In particular, we predict that either a two or three-stage process for MMB formation at HP is likely to occur in other group-15 (N, P) and -16 (O, S) elements, also in group-17 elements (Br, I), and in IV-VI and V_2-VI_3 compounds that are not PCMs at RP. A hint of these stages has been observed in GeSe and As_2S_3 at HP [84,87]. A more detailed discussion of the different stages of MMB formation in IV-VI and V_2-VI_3 compounds that are not PCMs at RP will be published elsewhere.

4. Nature of metavalent multicenter bonding

Once the mechanism of MMB formation in group-15 and -16 elements has been clarified, we will try to prove in this section that MMBs are equivalent to EDMBs and not to ERMBs, unlike previously suggested [59]. However, let us first summarize the available information on MMBs in group-15 and -16 elements and in PCMs.

Covalent bonds feature ES ≈ 2 and have a bond order of 1. In contrast, MMBs in PCMs and group-15 and -16 elements are characterized by smaller values of ES (≈ 1) and by longer bonds leading to a bond order of 0.5. On the other hand, molecules with EDMBs, such as diborane (B_2H_6) [168], and with ERMBs, such as I_3^-, are also considered to have a bond order of 0.5 [54,82], since bonds

in ERMBs and EDMBs are also longer than covalent bonds. Although ERMBs and EDMBs have a similar bond order, recent results of Wuttig and coworkers have shown that molecules with ERMBs, such as ClF_3, XeF_2, and SF_4, possess ES values higher than 1.5 [58]; i.e. similar to covalent bonds. Additionally, the absolute values of $\nabla^2\rho$ in molecules with ERMBs used to be positive and much larger [169] than those found in the MMBs in this and previous works [42,99]. However, the negative value of the ICOBI(3c) in PCMs and in group-15 and -16 elements has been previously interpreted as if the MMBs were ERMBs and not EDMBs since negative values of ICOBI(3c), although much larger, have been reported for molecules with ERMBs, such as XeF_2 [39].

To shed light on the above controversy regarding the possibility that MMBs could be either ERMBs or EDMBs, we have calculated the ES and ET values of some bonds present in different molecules and solids with known ERMBs and EDMBs (see **Fig. 11** and **Table S3** in ESI). The ES vs. ET values of the ERMBs and EDMBs of those molecules and solids are represented in **Fig. 6.** It can be observed that molecules with ERMBs, such as I_3^- and XeF_2, as well as solids with molecular solids in which there are ERMBs, such as linear I_3^- molecules in solid CsI_3 and cubic TeI_6^{2-} molecules in solid Cs_2TeI_6, exhibit larger values of ES and also of ET than MMBs. ERMBs are located in a yellow region above the red region of covalent bonds and much above that the green region of MMBs (see **Fig. 6**). This result agrees with Wuttig's calculations [58,170]. On the other hand, a molecule with EDMBs, such as B_2H_6, features an ES value somewhat smaller than those of MMBs in pnictogens and chalcogens and much smaller than ERMBs, but similar to ES values in lead halide perovskites with MMBs, such as $CsPbI_3$ [58,170]. Therefore, according to ES values it seems that MMBs are in the same green region of **Fig. 6** that EDMBs.

Regarding ERMBs and EDMBs, it must be considered that the large ET value in the studied molecules with ERMBs is indicative of the strong charge difference between the central and the external atoms of the linear 3c-4e bonds, in which external atoms have much larger negative charges than the central atom [169,171]. On the other hand, the low ES value (0.6) in B_2H_6, which has two B—H—B 3c-2e bonds can be understood if each 3c-2e bond is considered as the result of two resonant or interacting 2c-1e bonds, as already commented by Lipscomb and coworkers [172]. This consideration is similar to that of Wuttig and coworkers, who consider MMBs as 2c-1e bonds but without considering its multicenter character [58].

It was already suggested by Hoffmann and coworkers that Sb atoms in *sc*-Sb and in the planar Sb square array of $BaZnSb_2$ feature ERMBs [51]. However, we find, in a similar way as for *sc*-Sb, that Sb—Sb bonds in $BaZnSb_2$ (d=3.24 Å) have ET = 0 and ES = 1.16. These ET and ES values are closer to those of MMBs in PCMs and EDMBs in B_2H_6 than to those of ERMBs in I_3^- (see **Fig. 6**). Moreover, the bond distance is of the same order as that of the Sb—Sb bonds reported in *sc*-Sb at RP (d = 3.16 Å) [173] and much larger than the covalent bond of Sb in the A7 phase at RP (d = 2.96 Å). Therefore, we consider that Sb—Sb bonds in $BaZnSb_2$ are EDMBs. Our claim for EDMBs between Sb atoms of the square planar array in $BaZnSb_2$ is supported by Jeitschko and coworkers, who also suggested the presence of EDMBs with 0.5 bond order in As—As and Sb—Sb bonds in the square planar array of isostructural intermetallic compounds ACuAs$_2$ and AAgSb$_2$ (A= rare earth and uranium) [174]. Moreover, our claim for EDMB in $BaZnSb_2$ is also supported by Nesper, who suggested that Bi—Bi bonds at the square planar array of Bi atoms in the Zintl

phase of LiBi are 2c-1e bonds with 0.5 bond order [175]. Remarkably, the atoms in the square planar arrays of LiBi, $BaZnSb_2$, and $ACuAs_2$ and $AAgSb_2$ intermetallics show a square planar geometry as that of **Fig. 3b**, which is similar to that of the molecule XeF_4 with ERMBs.

All in all, we consider that both $BaZnSb_2$ and B_2H_6 mark the extremes of ET values (0 and 0.63) in the green region of **Fig. 6** that covers MMBs. The ET= 0 value for Sb—Sb bonds in $BaZnSb_2$ is a consequence of all Sb atoms in the plane array having the same electric charge (see **Fig. 11c**), which in turn is related to the translational symmetry since all Sb atoms in the planar array are equivalent (occupy the same Wyckoff *4c* site) [176]. It must be stressed that the presence of EDMBs in Zintl phases, intermetallic compounds, and cluster compounds (with homonuclear bonds) of maingroup elements is consistent with the well-known brittle and shiny metallic properties attributed to them [91,175,177]. Note that EDMBs bonds are directional bonds, due to the existence of partially localized electrons which lead to brittle behavior, and have delocalized electrons, thus leading to a shiny metallic aspect, as expected for incipient metals.

Another example of quasi-linear EDMB is found in Sb atoms in $SbPO_4$ [178]. In this compound (see **Fig. 11e**), P is fourfold coordinated to O atoms in a sp^3 geometry typical of ionocovalent bonds. However, Sb is fourfold coordinated to O atoms, with two short and two long Sb—O bonds, forming a see-saw geometry as that of **Fig. 3a** (note that Sb^{3+} has a single LEP). The two short (long) bonds have ES= 1.0 (0.8) and both have ET≈ 0.65 (in good agreement with the ionocovalent Sn—O bond since Sn and Sb are neighbor atoms). This means that the short (long) bonds are located in the regions of covalent (EDMB) in **Fig. 6**. In summary, we tentatively conclude that our calculations of ES and ET suggest that MMBs in the A_h and A_i phases of group-15 and -16 elements are equivalent to the EDMBs of boranes since they are in the same region of the 2D map of **Fig. 6**, which is separated from the region occupied by molecules and molecular solids with ERMBs. It is important to stress that our view is different to the previous belief that electron-deficient (-rich) elements could only form electron-deficient (-rich) multicenter bonds. Here we have shown that electron-rich elements, such as pnictogens, can form EDMBs in solids. The same is valid for chalcogens and halogens as we will show in a future paper where **Fig. 3** will be discussed in further detail.

The equivalence of MMBs and EDMBs is further supported by the mechanism of formation of the MMBs and EDMBs in contrast to that of ERMBs. The ERMB formation in I_3^- can be considered as the result of the approach of an I^- ion to an I_2 molecule (**Fig. 11a**) [49,81,83]. As they approach, a *trans influence* of the first unit into the second one occurred. According to the donor-acceptor charge-transfer model, a charge transfer from the donor unit (I^-) to the acceptor unit (I_2) occurs as they approach each other; in other words, the antibonding orbital of the covalent bond of the I_2 molecule is populated due to the LEP of the I^- ion. This *trans influence* occurs until both the intramolecular I—I distance of the I_2 molecule and the intermolecular I—I distance between the I^- ion and one of the I atoms in the I_2 molecule become almost equal [83]. The mechanism of ERMB formation can be also understood in the light of the σ-hole bond model [73,74,76–79]. In this model of secondary donor-acceptor bonds, the I^- ion with electronegative charge (nucleophilic) is attracted by the electropositive (electrophilic) region of the σ-hole (region of low electronic density) formed at the end of the I—I covalent bond of the I_2 molecule. When both electrophilic and nucleophilic regions approach, there is no charge transfer from the donor

to the acceptor unit, as claimed in the charge-transfer model, but simply a polarization of the charges in the I_2 molecule, which are induced by the approach of the I^- ion. This means that as the I^- ion approaches the closer I atom of the I_2 molecule, the ion shares part of its charge with the atom of the molecule and this sharing induces a shift of part of the charge of the closer I atom of the I_2 molecule towards the other I atom of the I_2 molecule, i.e. the I atom that is opposite to the I^- ion. This way the central I atom avoids severely violating the octet rule [72,73,79,179,180] and a symmetric (– + –) charge configuration is observed in the 3c-4e bond that explains the more electronegative external parts of this multicenter bond and also the large ET values of molecules with ERMBs. A similar procedure allows us to explain the linear ERMB formation and charge distribution in other linear molecules, such as XeF_2 and FHF^-. This bonding model is schematized in **Fig. 11a**. Therefore, it can be concluded that the ERMB formation does not involve a charge transfer between the primary and secondary bonds, as in MMBs, i.e. the primary bond in the ERMB does not lose charge, thus resulting in a rather large ES value compared to MMBs [58].

A completely different mechanism is found in the case of EDMB formation, e.g. in B_2H_6. This system can be considered as a two-proton attack on the B—B bond of the $B_2H_4^{2-}$ unit [181], but it can also be seen as two borane (BH_3) molecules with three covalent B—H bonds that interact together via secondary interactions in a dimerization process [182,183] . According to the σ-hole model of secondary interactions, a σ-hole appears at the end of each atom involved in the covalent bond and it becomes attracted by the large negative electrostatic potential at the BCP of one of the B—H bonds of the neighbor BH_3 molecule. Consequently, the two BH_3 molecules approach each other in such a way that there are two simultaneous *trans influences* between two intramolecular B—H bonds and two new intermolecular B—H bonds (see **Fig. 11b**). In these cases of *trans influence*, there must be a charge transfer of electrons from the two intramolecular B—H bonds towards the two intermolecular B—H bonds (note that neither B nor H atoms have LEPs that could provide the charge needed for the two new intermolecular bonds). This charge transfer or electron donation from the intramolecular B—H bonds towards the intermolecular B—H bonds leads to the conversion of two covalent B—H bonds (plus their associated weak secondary intermolecular bonds) into two B—H—B 3c-2e bonds, as suggested by Walsh [184]. The charge transfer ends when both intramolecular and intermolecular bonds become equal and the two B—H—B 3c-2e bonds are formed in the center of B_2H_6 (with all central B—H distances having the same length). The charge transfer from the intramolecular bond to the intermolecular one to form one B—H—B 3c-2e bond results in an ES < 1 for every central B—H pair. Moreover, it results in a considerable ET value (0.63) for every central B—H pair due to the different electronegativity of B and H atoms. Due to the *trans influence*, the lenghts of the central B—H units that form part of the B—H—B EDMBs become much larger than the external B—H covalent bonds in B_2H_6, thus explaining the 0.5 bond order of the EDMBs. The two simultaneous *trans influences*, leading to the formation of two *supported* 3c-2e bonds [54], are favored because of the filling of the empty sp^3 orbital of the two B atoms, so the B atoms in B_2H_6 reach a more stable tetrahedral geometry than the planar trigonal geometry of the BH_3 molecules (see **Fig. S14** in ESI) [183]. Moreover, the octet rule is accomplished for the B atom in B_2H_6, unlike in BH_3, if the two electrons of the B—H—B 3c-2e bond are considered to count for the external B atoms, as recently proposed [182].

The fundamental point is that the mechanism of EDMB formation in B_2H_6 is the same as that of MMB formation in the group-15 and -16 elements at HP, as shown in the previous section. In both cases, there is a charge transfer from the primary bond to the secondary one that softens and enlarges the primary covalent bond. The loss of charge of the primary covalent bond is the reason for the small value of ES in MMBs and EDMBs once they are formed. Curiously, this mechanism seems to be exactly the same mechanism of intermolecular, secondary bonding that occurs in the formation of polymeric CO_2 phases [163] and in the atomic/polymeric phases of elemental nitrogen and hydrogen at HP [88,147–150]. For instance, the *anomalous* increase (decrease) of the intramolecular (intermolecular) H—H distance in H_2 as pressure increases above 100 GPa is caused by the charge transfer from intramolecular to intermolecular bonds that ends once both bond distances equalize, and each bond in the atomic/polymeric phase has a single electron per atom pair, i.e. all H—H bonds are 2c-1e bonds [150]. Noteworthy, the charge transfer in hydrogen from the intramolecular H—H bond towards the intermolecular H—H bond is out of any doubt since the two electrons of the H_2 molecule at RP are between the two H atoms of the H_2 molecule and there is only one electron per H atom (no LEPs involved). Therefore, it seems that the atomic/polymeric phases (stage 3) of elemental hydrogen, supposed to exist above 500 GPa and discussed in the previous section, is also characterized by 2c-1e bonds, similar to EDMBs and MMBs.

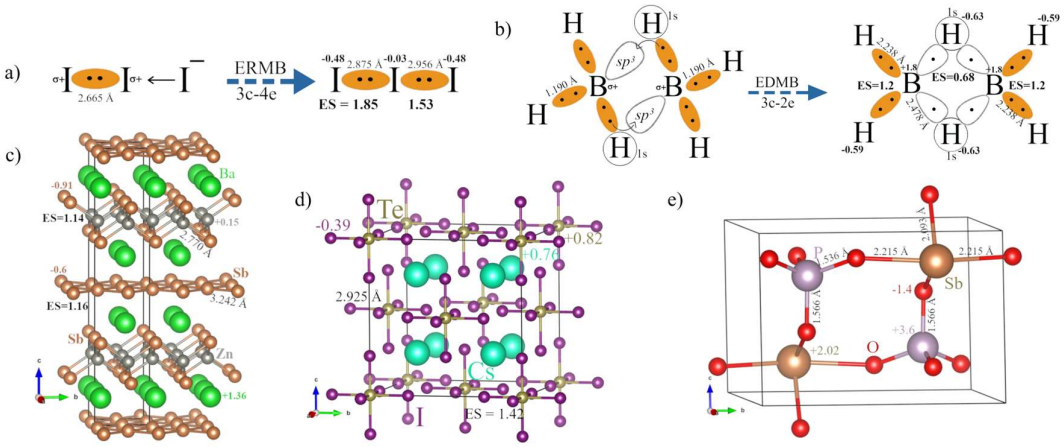

FIG. 11. The formation mechanism of a) I_3^- and b) B_2H_6 molecules are explored in the light of the σ-hole model for secondary bonds. c-d) The crystal structure of solids $BaZnSb_2$, Cs_2TeI_6, and $SbPO_4$ in the *bc* plane. Details on bond distances, atomic charges, ET, and ES of various bonds are illustrated here and summarized in **Table S3** in ESI.

Based on the above results, we suggest that MMBs in PCMs and the A_h and A_i phases of group-15 and -16 elements are equivalent to the EDMBs in boranes and also similar to those occurring in elemental nitrogen and hydrogen at HP once intermolecular and intramolecular bonds equalize [88,150]. Therefore, as previously mentioned for MMBs, the EDMB formation at HP in different elements, such as H, N, As, and Se, is characterized by a coexistence of localized and delocalized electrons [31] and is an intermediate step between covalent bonding, with fully localized electrons, and metallic bonding, with fully delocalized electrons. This view is consistent with the progressive delocalization of electrons as pressure increases until the metallic bond is reached at enough HP [31,88]. In this context, we consider that negative values of ICOBI(3c) found for MMBs in PCMs and group-15 and -16 elements, which have been interpreted as

indicative of ERMBs, could have been misinterpreted and should be thoroughly revised. Note that the negative values of ICOBI(3c) found in MMBs are close to zero, i.e. smaller in absolute value than those reported in molecules with ERMBs, like XeF_2 [39]. It is also important to stress that our results, which consider that MMBs in PCMs and in the A_h and A_i phases of group-15 and -16 elements are equivalent to EDMBs in boranes and also in the polymeric HP phases of nitrogen and hydrogen, are in contradiction with previous assumptions [88] that suggested that ERMBs should occur at HP for elements of groups 14-18 of the periodic table since typical hypervalent molecules with this kind of bond, such as I_3^-, XeF_2, XeF_4, and XeF_6 [81,82], correspond to elements of these groups. Note that the EDMB formation was previously assumed [88] to occur for elements of groups 1, 2, and 13 since they are present in typical molecules with this kind of bond, such as H_3^-, B_2H_6, and $Al_2H_7^-$ [54,61].

Additional support for the equivalence between MMBs and EDMBs comes from symmetry and energy arguments. According to Lubchenko and coworkers [31], the ERMB has been only observed in linear molecules with 3c-4e bonds since this is the only energetically stable configuration. The reason is that a system with *n* centers and (*n*+1) electrons is only stable if the *n*+1 electrons fill (*n*-1) localized molecular orbitals. This means that *n*+1 = 2(*n*-1), whose only solution is *n* = 3 [31]. This result agrees with simulations that showed the weak and easily perturbed bonds in the linear I_5^- molecule [171]. The above reasoning explains that ERMBs are mainly found in linear 3c-4e bonds in one, two, and three dimensions, e.g. in I_3^-, XeF_2, XeF_4, and XeF_6 molecules. These 3c-4e bonds can also be encountred in molecules inside solids, such as I_3^- in CsI_3 and TeI_6^{2-} in Cs_2TeI_6. In these two last compounds, Cs atoms give their electrons to the I_3 and TeI_6 molecular units to form I_3^- and TeI_6^{2-} molecular units that are linked to Cs atoms by ionic bonds. Our calculations confirm that ERMBs are located inside the molecular I_3^- and TeI_6^{2-} units. In CsI_3, $Cs^{0.27+}$ atoms give charge to the three I atoms of the I_3^- molecule that show different negative charges similar to those of **Fig. 11a**. Note that in the I_3^- units of CsI_3 at RP, there are two slightly different I—I bonds (one short and one large) that tend to form two equal ERMBs at HP as shown by the linear array in **Fig. 3a** [185]. On the other hand, the atomic charge in Cs_2TeI_6 is distributed as: $Cs^{0.76+}$, $Te^{0.80+}$, and $I^{0.39-}$. This means that the TeI_6^{2-} units (see **Fig. 11d**), which form a cubic array as in **Fig. 3c**, have a Te atom that also gives almost one electron to the I atoms. Therefore, as expected for linear 3c-4e ERMBs (in this case in three perpendicular directions), the external I atoms concentrate the electronic charge, so this cubic TeI_6^{2-} unit behaves as a pseudo-SbI_6^{3-} unit that is isoelectronic to XeF_6; a molecule that also exhibits one of the two geometries in **Fig. 3c** [186].

From symmetrical arguments, the equivalence of MMBs and EDMBs comes from the impossibility of the occurrence of ERMBs in extended solids. According to Lubchenko and coworkers [31], the multicenter bond becomes electron deficient for any molecule longer than three centers, so the only possible kind of multicenter bonding in extended chains and solids is the EDMB. This is especially clear in crystalline solids, e.g., $BaZnSb_2$ and As-II, due to the existence of translational symmetry. As already mentioned, all Sb atoms at the planar array in $BaZnSb_2$ are at *4c* sites, so they are all equivalent and must have the same charge ($Sb^{0.6-}$) [176]. Similarly, all As atoms in the *sc* phase of As-II are located in the *4a* Wyckoff position, so all atoms are equivalent and must have the same charge. In both examples ET = 0, so no ERMBs with high values of ET as those shown in **Fig. 6** can be formed by As and Sb atoms in these two solids. The

translational symmetry in solids makes it impossible for the central atom of a given hypercoordinated unit in **Fig. 3** to shift electronic charge to the external parts of the unit, as it happens in molecules with ERMBs, in which the central atom has always a positive charge because this will require the existence of different Wyckoff sites for the central and external atoms of the smallest trimer molecule represented in **Fig. 3**. Different charges for different Wyckoff sites occur for instance in β-GeTe with *rs* structure because Ge and Te are in *4a* and *4b* sites. Assuming that one of the two elements will have a positive charge and the other one a negative one, let us take δ, 3c-4e bonds along three perpendicular axes with cubic symmetry as shown in **Fig. 3c**, could be possible around the positive ion with a $Te^{\delta-}$—$Ge^{\delta+}$—$Te^{\delta-}$ configuration according to our reasoning of charge distribution (– + –) in the I_3^- molecule, but not around the negative ion with $Ge^{\delta+}$—$Te^{\delta-}$—$Ge^{\delta+}$ configuration. On the other hand, no five-center bond with $Te^{\delta-}$—$Ge^{\delta+}$—$Te^{\delta-}$—$Ge^{\delta+}$—Te^{δ} configuration or larger ERMBs with equal Ge—Te bond distances could be possible because the central atoms in molecules with ERMBs should exhibit the more positive charges [171] due to the *trans influence*. It must be noted that linear or quasi-linear ERMBs larger than three centers (4c-6e, 5c-6e, 5c-8e, etc.) have been thoroughly studied, but they do not have the equal or nearly equal bond distances in EDMBs and 3c-4e bonds [171,187]. The situation is different in molecules, even inside solids, where such symmetry restrictions must not be obeyed. One example is the recent finding of ERMBs in the low-temperature monoclinic phase of crystalline RuP, where linear 3c-4e bonds have been found in molecular Ru-Ru-Ru units (the central and external Ru atoms of the trimer occupy different *4e* Wyckoff sites) along zigzag-like ladders [188]. Therefore, we consider that ERMBs with equal bond distances are not possible in linear molecules of more than three atoms inside crystalline solids, thus MMBs in solids cannot be equivalent to ERMBs.

It could be argued against our claim for the equivalence between MMBs and EDMBs that linear EDMBs are rare in molecules, whereas linear 3c-4e ERMBs, such as those of **Fig. 3**, are common in molecules [61]. In this regard it must be emphasized that there are two types of 3c-2e bonds: supported and unsupported 3c-2e bonds [54]. The EDMBs of H_3^+ and B_2H_6 are of supported type and tend to be bent; however, the EDMBs in PCMs and the A_h and A_i phases of group-15 and -16 elements are of unsupported type, such as the B—H—B and Al—H—Al bonds in $B_2H_7^-$ and $Al_2H_7^-$. It has been proposed that these unsupported bonds can be either bent or linear; bent in the absence of a crystal lattice and linear when the crystal lattice is present [189,190]. Therefore, the existence of linear unsupported EDMBs in crystalline solids is justified due to the presence of the translational symmetry of the crystal lattice. These reasonings allow us to tentatively propose that MMBs with the geometries of **Fig. 3** are likely the typical EDMBs in solids.

It is significant that the occurrence of EDMBs under compression, as in the A_h and A_i phases of group-15 and -16 elements, in atomic/polymeric nitrogen and hydrogen, and, in general, in all materials at elevated pressures, agrees with the general view that all elements, irrespective of their valence electrons, should show EDMBs at HP [31,90]. Note that pressure tends to increase atomic coordination and all elements and compounds will fall short in electrons to share with neighbor atoms at a certain pressure, i.e. above a given atomic coordination [88]. Therefore, all the new bonds in hypercoordinated atoms will have to share necessarily less than two electrons per atomic pair until full electron delocalization, typical of metallic bonding, is finally attained at even higher pressures.

To close this paper, we want to make a final observation on the hypercoordinated multicenter units shown in **Fig. 3** that we have previously cited in a cursory way regarding the different geometrical units that have been experimentally observed upon formation of both ERMBs and EDMBs in electron-rich elements, such as those of groups 15 and 16 [191–193]. Note that the geometries in **Fig. 3** (in most cases related to the presence of LEPs) are different to those found in EDMBs of electron-deficient elements, such as group 13 and hydrogen, which have no LEP. It has been many times discussed in the literature that hypervalent molecules of main-group elements do not obey the 8 – *N* rule for atomic coordination, where *N* is the total number of valence *s* and *p* electrons [191–193]. In other words, hypervalent molecules show a higher coordination (hypercoordination) than initially expected if all bonds were considered single covalent 2c-2e bonds. The violation of the 8 − *N* rule has been many times interpreted (e.g. Ref. [44,194]), as if these hypercoordinated molecules, with assumed 2c-2e bonds, would have violated the doublet/octet rule of Lewis [195]; i.e. it has been considered that each atom is surrounded by more than the two (eight) atoms allowed for *s* (*s* and *p*) orbitals. On the other hand, several works have discussed that hypervalent molecules do not violate the doublet/octet rule [79,179,196–202]. On the other hand, it has also been commented that the octet rule can be violated in hypervalent units [194]. In many of these works, it has been proposed that the terms "hypervalence" and "hypervalent" should be sent to the graveyard and replaced by more convenient terms, like "hypercoordinated" or "hypobound" [179,194,196–202].

Recent works of Grabowski on molecules have shown the process of formation of hypervalent units due to different kinds of non-covalent interactions in secondary bonds, such as hydrogen, triel, tetrel, pnictogen, chalcogen, and halogen bonds, and have also pointed out that the mechanism of formation of these secondary bonds is the same [77,79]. Moreover, it has been suggested that the hypervalent units formed by secondary bonds, leading to 3c-4e ERMBs in molecules follow the rules of the VSEPR model [43,44,203]. Since the ERMBs have not been clearly distinguished in the diagrams of the hypervalent units in previous works [43,44,77,79], we have plotted in **Fig. 3** the simplest hypercoordinated units with ERMBs according to the VSEPR model [203]. Curiously, some of the hypercoordinated units of **Fig. 3a**, initially deduced for ERMBs, have been found to agree with those experimentally observed in amorphous and crystalline GST [43,44], and we have shown that the hypercoordinated units of crystalline GST as a PCM can be considered to have EDMBs. Moreover, we have shown that other hypercoordinated units, such as those formed by the Sb atoms in $SbPO_4$ (**Fig. 3a**), those formed by Sb atoms in the square planar array of Sb atoms in $BaZnSb_2$ (**Fig. 3b**), and those of the A_h and A_i phases of group-15 and -16 elements (**Fig. 3c**), also correspond to linear EDMBs. In view of these results, we tentatively conclude that the hypercoordinated multicenter units plotted in **Fig. 3** correspond to the simplest linear multicenter bonds that fulfill the VSEPR rules, irrespective of whether they are ERMBs (3c-4e) or EDMBs (3c-2e). In those hypercoordinated units, multicenter bonds can be directed along one, two, and three dimensions, alone or in combination with LEPs and ionocovalent bonds. Moreover, since our work shows that linear hypercoordinated multicenter units occur for both ERMBs and EDMBs in molecules and solids, we suggest, in agreement with previous works [179,196–202], that the "hypervalent" term should be replaced by "hypercoordinated", as shown in **Fig. 3**.

In order to avoid misinterpretation of **Figs. 3** and **7a-c**, it is important to stress, for the case of solids, that the hypercoordinated multicenter units in **Fig. 3** could be extended or replicated along the three spatial dimensions, e.g. the case of the rhombohedral and cubic units of the A_h and A_i phases of group-15 and -16 elements schematically represented in **Fig. 3c**. The same extension to 3D must be also understood in relation to the sequence in **Fig. 7a-c**. For instance, one primary covalent As—As bond in As-I is almost linearly linked (secondary bond) to two As atoms of neighbor layers (As···As—As···As) along one direction; thus, the *trans influence* of the two As···As secondary bonds on the primary covalent As—As bond is on both sides of the As_2 molecule. Moreover, since each As atom in As-I participates in three, almost perpendicular primary As—As bonds, this picture should be extended in the three, almost perpendicular directions. Consequently, extended 3D EDMBs are formed, leading to the A_h phase of As-II at HP, and not 3c-4e bonds, as previously assumed [61], and as **Fig. 7a-c** could initially suggest due to its limited, schematic view.

Here we propose a new notation for the hypercoordinated multicenter units formed by electron-rich elements in **Fig. 3**. Our notation is different from that used by Crabtree [81] and Grabowski [79], who use the number of ligands, L, that can be understood as the number of bonds, but do not distinguish between ERMBs and EDMBs since previous diagrams. This can be understood because they only considered that linear hypercoordinated multicenter units only applied to ERMBs. The hypercoordinated multicenter units of **Fig. 3** can be notated as A(C,E,M), where A refers to the hypercoordinated central atom A and C, E, and M refer to the number of covalent bonds, LEPs, and multicenter bonds (both ERMBs of EDMBs), respectively.

To exemplify the use of our notation with several compounds featuring EDMBs, we can cite: i) the A(0,3,1) unit of chains of Sb atoms in Li_2Sb [51]; ii) the A(1,2,1) unit of O atom in SbOF [204]; iii) the A(2,1,1) unit of Sb atoms in $SbPO_4$ and of Sb atoms in SbOF; iii) the A(3,0,1) units of P atoms in $TiPO_4$-V at 48 GPa [205]; iv) the square planar A(0,2,2) unit of Sb atoms at the planar array in $BaZnSb_2$; v) the square pyramidal A(1,1,2) units present around Tl and I atoms in TlI; and vi) the rhombohedral and cubic A(0,1,3) units of the A_h and A_i phases in group-15 and -16 elements as well as of many PCMs of IV-VI and V_2-VI_3 families with *rs* and tetradymite structures, respectively, including crystalline GST. We would like to add the A(0,0,1) unit (not shown in **Fig. 3** but it is similar to the A(0,3,1) unit without the three LEPs) which is the type of bond in atomic/polymeric hydrogen at HP [205]. A more detailed discussion of these and other compounds with EDMBs that show the geometries described in **Fig. 3** will be published elsewhere.

As a first approximation, we can consider that in the A(C,E,M) units of **Fig. 3**: i) each covalent bond contains two electrons; ii) each LEP contains two electrons; and iii) each multicenter bond is characterized by sharing two electrons between every two atoms (ERMB) or only one electron between every two atoms (EDMB). This means that, in general, the geometric A(C,E,M) units of **Fig. 3** for EDMBs seem to satisfy the octet rule. This is not so clear for ERMBs [194], despite Grabowski has reasoned that the formation of the hypercoordinated units in molecules with ERMBs [77,79] is connected with the mechanism of the σ-hole model to preserve the doublet rule of group-1 and -2 elements and the octet rule in main-group elements [79,179]. Since this work is devoted to MMBs, which we have proposed to be equivalent to EDMBs, the violation or

not of the octet rule in hypercoordinated units with ERMBs is not going to be further discussed in this paper.

Regarding EDMBs, it seems that the octet rule seems to be satisfied in molecules [182] and the same is expected in solids. Taking into account the above considerations, eight electrons seem to surround each A atom in hypercoordinated units with only one EDMB (1D geometry), such as in the A(0,3,1), A(1,2,1), A(2,1,1), and A(3,0,1) units of **Fig. 3a**. The same occurs for the units with two EDMBs (2D geometry), the A(0,2,2), A(1,1,2), and A(2,0,2) units of **Fig. 3b**, and for the units with three EDMBs (3D geometry), such as the cubic A(0,1,3) units of **Fig. 3c**. A clear example of the validity of the octet rule in the A(0,1,3) unit is the A_h phase of group-15 elements. Group-15 elements have two *s*-type and three *p*-type electrons. In the A_h phase, the *s*-type electrons form part of the inactive LEP and are distributed into six lobes, as shown in the cubic A(0,1,3) unit of **Fig. 3c**, while the three *p*-type electrons participate in the three mutually perpendicular EDMBs. Therefore, the central A atom of the A(0,1,3) units has valence eight electrons, thus satisfying the octet rule. This result is contrary to the previous assumption that hypercoordinated units in MMBs led to a violation of the octet rule [44].

The same reasoning would apply to consider the validity of the doublet rule for H, when it forms EDMBs at HP. In particular, polymeric H (…H—H—H…) at HP [150] could be considered as a hypercoordinated A(0,0,1) unit (with no LEPs) with only one EDMB (1D geometry). Therefore, two electrons surround each H atom. In the end, assuming that each covalent bond, each LEP, and each EDMB, accounts for two electrons in multicenter hypercoordinated A(C, E, M) units, the doublet or octet rule is satisfied for the central atom A taking into account that 2(C+E+M) = 2 or 8. For the doublet rule, it has to be satisfied that C+M = 1 since in this case there is no LEP (E = 0). Therefore, H has only two possibilities, either it has only a covalent bond as in H_2 or it has only an EDMB as in atomic/polymeric H at HP. For the octet rule, it has to be satisfied that C+E+M = 4. This is exactly the condition met by all the A(C,E,M) units in **Fig. 3**.

Interestingly, the octet rule seems to be violated in the hypercoordinated units with EDMBs for group-16 elements, e.g. the cubic and rhombohedral A(0,1,3) units of α-Po and β-Po. In this case, in addition to the six *p*-type electrons of the three EDMBs around each central A atom (three coming from the central atom), one has to count the three additional electrons of the A atom (two *s*-type electrons corresponding to the LEP plus the extra *p* electron in chalcogens compared to pnictogens). These extra electrons are distributed: i) among the six lobes of the cubic A(0,1,3) unit (**Fig. 3c**), as previously noted for α-Po, or ii) in the toroidal pink halo (monosynaptic basin) of the rhombohedral A(0,1,3) unit (**Fig. 3c**) typical of β-Po. Therefore, a total number of nine electrons seems to be around each hypercoordinated EDMB unit for chalcogens, thus violating the octet rule. Curiously, the prevalence of the cubic vs. the rhombohedral units in AF_6E molecules (A is the central atom, F is the ligand atom and E is the LEP) with ERMBs, such as XeF_6, has been already studied [206]. It has been concluded that AF_6E molecules with both the cubic O_h symmetry, like that of the cubic unit of **Fig. 3c**, or the C_{3v} symmetry, like that of the rhombohedral unit of **Fig. 3c**, are very close in energy. The predominance of one geometry over the other seems to be related to a very fine balance between ligand-ligand repulsions and the energy gained by the expansion of the two nonbonding electrons of the LEP in the valence shell that mainly depends on the atomic radii ratio between the central atom and the ligands.

Interestingly, the small energy difference between the two configurations for AF_6E molecules with ERMBs is similar to that we find between the two polymorphs of Po at 0 K, which explains that β-Po tends to α-Po above 2 GPa. Therefore, we can speculate that, similarly to the case of molecules with ERMBs [206], the cubic and rhombohedral configurations of Po likely occur because of the fine balance of the two above mentioned energy terms that depend on temperature and pressure. Moreover, it has been suggested that the electrons not involved in bonding in AF_6E molecules with ERMBs and being part of the LEP could behave as a mixture of valence-core electrons, so that on average they contribute with only two valence electrons [206]. Therefore, it can also be speculated that the three extra electrons, which are not directly involved in the three EDMBs of chalcogens, likely behave in a similar way, so that on average they contribute with only two valence electrons, that summed to the other six *p*-type electrons of the three EDMBs make the central atom to satisfy the octet rule. The mixture of valence-core electrons for *s*-type electrons can be justified in the A_h and A_i phases of group-16 elements because of the large energy difference between *s* and *p* states in chalcogens [142].

As a summary of this section, we conclude that the MMBs are equivalent to EDMBs since both bonds are described by interacting 2c-1e bonds (multicenter bonds). In fact, it can be considered that the MMBs with the linear or quasi-linear geometries presented in **Fig. 3** are the type of unsuported EDMBs that typically occur in solids. We have shown that other compounds, such as $SbPO_4$ or $BaZnSb_2$, this last previously assumed to exhibit ERMBs [51], are also characterized by EDMBs in one and two dimensions, respectively, that add to the EDMBs in three dimensions found in the octahedrally-coordinated phases of pnictogens and chalcogens. We have also proposed that the above mentioned EDMBs seem to be the same type of bond in atomic/polymeric nitrogen and hydrogen at HP since the mechanism of formation of the secondary, intermolecular bonds is the same for nitrogen, hydrogen, B_2H_6, and MMBs in group-15 and -16 elements as well as in PCMs. These examples contrast with materials with ERMBs that not only are located in a different position in the 2D ES vs. ET map, but also show a completely different mechanism of formation. We have additionally justified that in extended solids hypercoordination is only possible for EDMBs since ERMBs can only be formed in molecular solids due to energetic and symmetry restrictions. We have shown that linear or quasilinear hypercoordinated multicenter units (both with ERMBs and EDMBs) around a central A atom have geometries compatible with the VSEPR theory and are not hypervalent. We suggest that the "hypervalent" units should be renamed as "hypercoordinated multicenter units" and propose a minimum set of linear multicenter bonds for atoms with *p*-type orbitals in **Fig. 3** with a notation to understand the geometry of the different hypercoordinated multicenter units. Finally, we have reasoned that the doublet/octet rule is satisfied around the central A atom in hypercoordinated units with EDMBs.

5. Conclusion

To study the mechanism of formation and nature of MMBs, we have performed systematic theoretical work on group-15 and -16 elements, the simplest materials undergoing a change from the pre-MMB to the MMB scenario by the effect of pressure or the change in composition by heavier elements. We have used some bond descriptors, previously used by researchers defending either the metavalent or multicenter models of the bond in PCMs, as well as the bond and band pictures. In particular, we have deeply studied how pressure decreases the octahedral

distortion of the trigonal *R*-3*m* (A7) and trigonal $P3_121$ (A8) crystalline structures of group-15 and -16 elements at RP, respectively, and the A_h (*sc*) and A_i phases of α-Po and β-Po, respectively. As a result, we conclude that:

1. The A7 structure of group-15 (As, Sb, Bi) elements tends at HP towards the A_h phase of α-Po at RP, while the A8 phase of group-16 (Se, Te) elements tends at HP towards the A_i phase of β-Po at RP. These results are consistent with the observation of α-Po and β-Po as HP phases in group-15 (P, As) and group-16 (S, Se, Te) elements, respectively, and agree with the electron count of Papoian and Hoffmann on the formation of hypercoordinated units [51]. The formation of the cubic α-Po structure in group-15 elements is favored by their five valence electrons, while the formation of the rhombohedral β-Po structure in group-16 elements with six valence electrons occurs because the extra valence electron avoids the complete inactivation of the LEP at HP and induces a distortion in the cubic structure. The reason why α-Po occurs at RP and low temperatures could be related to the small ligand-ligand repulsion between Po atoms at low temperatures compared to the energy gained when the LEP is promoted to the valence shell.

2. Unconventional MMBs, as those present in PCMs and that we propose to be equivalent to EDMBs, are present in both the octahedrally-coordinated HP A_h and A_i phases of group-15 (As, Sb, Bi) and -16 (Se, Te) elements, respectively. Since these HP phases are not experimentally found in some of these elements, our results must be reinterpreted in a more general way: group-15 and -16 elements change in bonding from covalent *ppσ*-bonds plus secondary bonds to EDMBs as the octahedral atomic coordination is approached on increasing pressure. In particular, we propose that fully developed EDMBs occur in As-II above 25 GPa, in Sb-II above 8 GPa, in Bi-III above 2.7 GPa, in Se-V above 40 GPa, and Te-III above 8 GPa. Additionally, we propose that a mixture of covalent and EDMBs or even asymmetric EDMBs could also occur in intermediate HP phases, such as Bi-II above 2.5 GPa (Bi-II), in Se above 23 GPa (Se-III and Se-IV), and in Te-II above 4 GPa.

3. Polonium, in its two polymorphs at RP (α-Po and β-Po), is the only element, together with tetragonal boron [27], that exhibits EDMBs at RP. Remarkably, Po is the only element with all bonds being fully EDMBs at RP, unlike tetragonal boron, which exhibits a mixture of EDMBs and covalent bonds. Since EDMBs are softer than covalent bonds, one can understand the low melting temperature of Po, which has been considered a common metal or semimetal, despite it displays the octahedral coordination of incipient metals [13].

4. In general, EDMBs occur at smaller pressures along the series Se-Te-Po and As-Sb-Bi. This means that the effect of pressure is equivalent to the substitution of the composition of elements by their heavy analogs. This result is consistent with the larger distortion of octahedral coordination for the lighter elements, i.e. those with stronger LEP stereoactivity. It is also consistent with the well-known effect that pressure is equivalent to going down the group in the periodic table since pressure induces a decrease of the LEP stereoactivity in the same way as going down the group to heavier elements. Therefore, both pressure and composition tend to transform covalent *ppσ*-bonds into EDMBs and finally into metallic bonds. Interestingly, both pressure and composition lead to an increase in mass density, which in turn results in an increase in electronic density. Therefore, other ways of increasing electronic density could also lead to a

decrease in the LEP stereoactivity and the formation of EDMBs. Two examples are chemical pressure [207] and reduction, i.e. providing electrons to the system [51].

5. EDMBs can be potentially observed in all materials that show at RP a mixture of primary covalent *ppσ*-bonds and secondary bonds in which LEPs are involved. Consequently, our results can be readily extrapolated to all groups 15, 16, and 17 elements (including N, O, and F). In particular, EDMB formation will occur in phosphorous at the A7-to-A_h PT experimentally reported at HP [104,208], and N could form EDMBs at pressures higher than those for which the black-P structure is found [209]. Finally, sulfur will start showing some EDMBs in S-III or S-IV phases above 30 GPa since these phases exhibit positive pressure coefficients of all Raman-active modes [131], although the A_i phase is reported in S-V above 150 GPa [121]. In addition, the observation of EDMBs is also expected in hydrogen above 500 GPa. In this context, it must be mentioned that since EDMB is characterized by a mixture or coexistence of localized and delocalized electrons, in general, EDMBs are expected to be found in many materials at sufficiently high pressures as a prior step to full electron delocalization corresponding to the metallic bond.

Our results can also be extrapolated to other families of materials with covalent *ppσ*-bonds and LEPs, such as binary IV-VI and V_2-VI_3 families and related ternary compounds that are, in turn, related to PCMs. Moreover, we propose that EDMBs could also be found in compounds with *p*-type covalent bonds in which cations show the presence of LEPs (typical of elements at their smallest valence state), such as Cl^{5+}, Br^{5+}, I^{5+}, S^{4+}, Se^{4+}, Te^{4+}, As^{3+}, Sb^{3+}, Bi^{3+}, Ge^{2+}, Sn^{2+}, Pb^{2+}, Ga^{+}, In^{+}, and Tl^{+}. The EDMB formation in these compounds at different pressures will depend on the strength of the LEP stereoactivity at a given electronic density. EDMBs will be formed at RP when LEP stereoactivity is negligible, but they will not be formed when LEP stereoactivity is strong. This consideration agrees with the results of Waghmare et al. [30] and is also consistent with the decrease of LEP stereoactivity for a given cation, e.g., Sn^{2+}, Sb^{3+}, when linked to chalcogen atoms in the series S-Se-Te [210]. This explains why PCMs at RP are observed mainly in Te-based compounds, e.g., in SnTe and Sb_2Te_3 at RP, and not in SnS, SnSe, Sb_2S_3, and Sb_2Se_3 at RP. In these last compounds, EDMBs will be formed at HP, as already proved for GeSe, which is isostructural to SnS and SnSe [84]. It is also well known that cation LEP stereoactivity decreases along a group, e.g. along the series Ge-Sn-Pb or As-Sb-Bi. Therefore, EDMBs are only encountred, for instance, in Se-based compounds PbSe and Bi_2Se_3 at RP and not in GeSe, SnSe, As_2Se_3, and Sb_2Se_3 at RP; however, EDMBs will be formed in these last compounds at HP, as already proved for GeSe [84] and As_2S_3 (isostructural to As_2Se_3) [87].

6. The formation of EDMBs with increasing electronic density proceeds in a gradual, similar way in both group-15 and -16 elements. This result is in line with previous suggestions that proposed the formation of multicenter bonds by the increase in mass density, e.g. by increasing pressure [31,89]. Notably, we have shown that the mechanism of EDMB formation proceeds via different stages that depend on the type of LEP involved in the secondary bonds. In group-16 elements (with a *p*-type LEP involved in secondary bonds), the mechanism of EDMB formation comprises two stages, while in group-15 elements (with an *s*-type LEP involved in secondary bonds the mechanism comprises three stages. We suggest that these mechanisms could be universal, at least, in *p*-type elements, and that all materials undergoing a bonding change from a covalent

ppσ-bond plus a secondary bond to an EDMB upon increase of electronic density will follow a two- or three-stages mechanism depending on the type of LEP involved in secondary bonds. In particular, we predict that EDMB formation in group-17 elements (Br and I) will proceed via a two-stage mechanism due to the *p*-type LEPs present in these elements at RP. In more complex compounds, such as IV-VI and V_2-VI_3 compounds, the presence of two or three phases must be further clarified. We have also shown that these stages show a parallelism with the molecular, semimolecular, and atomic/polymeric stages in nitrogen and hydrogen at HP.

7. The formation of MMBs in group-15 and -16 elements either at RP or at HP is in good agreement with the 2D map showing the number of electrons shared (ES) vs. the normalized number of electrons transferred (ET) used by Wuttig and coworkers to classify bonds in materials [69]. By calculating the ES and ET values of different materials with MMBs, either ERMBs or EDMBs, we have shown that these two multicenter bonds are located in different positions of the map, so the ES and ET values calculated with QTAIM theory seem to be valid to explain the different types of bonds in materials (in particular group-15 and -16 elements) that occur under compression and upon change of composition.

Moreover, by working with elemental solids exhibiting pure covalent bonds, we show that EDMB can occur between purely covalent and metallic bonds. This is in contrast to a previous claim that considered that the formation of multicenter bonds could only occur between ionic and metallic bonds [31]. It can be concluded that EDMB is an unconventional bond characterized by a mixture of localized electrons between two atoms and delocalized electrons over more than two atoms. This means that EDMBs can be considered as 2c-1e bonds that are characterized by ES ≈ 1; i.e. half the value expected for a pure covalent bond. In conclusion, the EDMB is a directional bond intermediate between ionocovalent *p*-type bonds (with fully localized electrons) and metallic bonds (with fully delocalized electrons), where the number of electrons shared between two atoms is around one instead of two as in ionocovalent bonds.

8. The EDMBs in solids will be easily recognized by the scientific community if clear observables are defined for incipient metals. We have proposed that one of the easiest ways to evidence the change from the pre-MMB scenario to the MMB scenario at HP is by detecting the *normal* hardening of the previous soft optical modes observed in covalent *ppσ*-bond materials. This will occur simultaneously with a *normal* decrease of the bond distance as expected in stage 3 of the mechanism of EDMB formation. In this sense, we have come up with the idea that soft optical modes in *p*-type materials are the signature of the instability of the ionocovalent *ppσ*-bonds at HP, in a similar way as soft acoustic modes at the Brillouin zone edges are the signature of the instability of ionocovalent $sp^3\sigma$-bonds. Additionally, we have commented that EDMBs are longer than covalent bonds. It has been estimated that EDMBs are 1.2 to 1.3 times larger than covalent bonds at the same pressure/temperature conditions. On the other hand, EDMBs have ca. half the electronic charge of covalent bonds since they have *ca.* half ES values, thus EDMBs should have typical charge densities 60 to 65% smaller than covalent bonds. These descriptors can help researchers identifying EDMBs in solids. For instance, formation of EDMBs is expected to occur in iodates at HP since recent studies have evidenced the equalization of the short and long I—O bonds with increasing pressure that are concomitant with the softening of high-frequency optical phonons [211–213].

9. Based on ES values (ES ≈ 1), on the mechanism of MMB formation, and energy and symmetry arguments, we have shown that MMBs in PCMs and group-15 and -16 elements are equivalent to the EDMBs of diborane and of atomic/polymeric nitrogen and hydrogen at HP, despite in these materials there could be no LEPs and even no *p*-type electrons. In addition to molecules, we have shown that EDMBs are also present in solids as extended linear chains of hypercoordinated atoms along one, two, and three directions. For instance, we have reasoned it for several solids: $SbPO_4$ (1D), $BaZnSb_2$ (2D), and the A_h and A_i phases of group-15 and -16 elements (3D). Some of these examples were previously assumed to exhibit ERMBs. The MMB is thus not equivalent to ERMB; a bond present in hypercoordinated molecules, such as I_3^-, XeF_2, XeF_4, XeF_6, and in molecular solids, such as CsI_3 and Cs_2TeI_6, but not forming extended chains in solids neither in one, two, nor three dimensions. The similarity between MMBs and EDMBs and the dissimilarity with ERMBs is patent in the ES vs. ET map.

10. Units with linear or quasi-linear ERMBs or EDMBs fulfill the VSEPR theory. In all of them, the 8 − *N* rule is not obeyed but the doublet/octet rule is in general satisfied for EDMDs. We have proposed that "hypervalent units", in which linear or quasi-linear ERMBs or EDMBs in one, two, or three dimensions are present, should be renamed as "hypercoordinated multicenter units". Moreover, we have suggested a new notation for these hypercoordinated units based on the number of ionocovalent bonds, LEPs, and multicenter bonds.

Finally, it must be stressed that the results of this work have very far-reaching consequences for the broad scientific community, especially for condensed matter scientists: i) they provide a comprehensive framework to understand how the 3c-2e bonds and in general EDMBs are formed in solid elemental and complex materials from primary ionocovalent *ppσ*-bonds plus secondary bonds involving LEPs and even in atomic/polymeric nitrogen and hydrogen (the last one with no *p* electrons), thus providing a new paradigm for describing many structures; ii) they show several descriptors that can be used to identify EDMBs at RP and HP in a wide variety of materials from simple elements to complex materials, such as PCMs, highly efficient thermoelectrics, and topological insulators, superconductors, and highly efficient photovoltaic materials; and iii) they open the door for a better understanding of the chemical bonding mechanisms in the above commented advanced materials for improving their performance [159]. Additionally, we hope that this work will promote: i) further work to understanding EDMBs in solids and their associated exceptional property portfolio; and ii) a revision that helps to unify the notation, among the condensed matter physicists, chemists, and materials scientists of this well-known unconventional bond in molecules, but rather poorly known in solids.

Supplementary information

The Supporting Information is available free of charge on the website.

Acknowledgments

This publication is financed by Spanish Ministerio de Ciencia e Innovación and the Agencia Estatal de Investigación MCIN/AEI/10.13039/501100011033 as part of the project MALTA Consolider Team network (RED2022-134388-T), and I+D+i projects PID2019-106383GB-42/43,

PGC2021-125518NB-I00, and PID2022-138076NB-C42/C44 co-financed by EU FEDER funds, by project PROMETEO CIPROM/2021/075 (GREENMAT) financed by Generalitat Valenciana, and by project AYUD/2021/51036 financed by Principality of Asturias (FICYT) and co-financed by EU FEDER. This study also forms part of the Advanced Materials programme supported by MCIN with funding from European Union NextGenerationEU (PRTR-C17.I1) and by Generalitat Valenciana through project MFA/2022/025 (ARCANGEL), and by Principality of Asturias (FICYT) through project TED2021-129457B-I00. AOR also thanks the Spanish MINECO for a Ramón y Cajal fellowship (RyC-2016-20301).

We would like to express our gratitude to Jose Manuel Recio, Juan Ángel Sans, Álvaro Lobato, Julia Contreras-García, David Santamaría-Pérez, Maria Consuelo Jiménez-Molero, and Ángel Vegas for their insightful and engaging discussions on our findings. Their input and feedback greatly enriched the development of this article. Particularly, we want to acknowledge Álvaro Lobato and Julia Contreras-García, who made us aware of the paralelism between the mechanism of MMB formation and the formation of atomic/polymeric phases in nitrogen and hydrogen, respectively.

References

[1] J.K. Burdett, Chemical Bonding in Solids, Oxford University Press, New York, 1995.

[2] P. Ball, Nature 469 (2011) 26.

[3] G. Frenking, S. Shaik, The Chemical Bond, Wiley-VCH Verlag, Weinheim, Germany, 2014.

[4] S. Alvarez, R. Hoffmann, C. Mealli, Chem. Eur. J. 15 (2009) 8358–8373.

[5] P. Needham, Stud. Hist. Philos. Sci. A. 45 (2014) 1–13.

[6] A.E. Reed, L.A. Curtiss, F. Weinhold, Chem. Rev. 88 (1988) 899–926.

[7] G.H. Wannier, Phys. Rev. 52 (1937) 191–197.

[8] N. Marzari, A.A. Mostofi, J.R. Yates, I. Souza, D. Vanderbilt, Rev. Mod. Phys. 84 (2012) 1419–1475.

[9] B. Silvi, A. Savin, Nature 371 (1994) 683–686.

[10] A. Lobato, H.H. Osman, M.A. Salvadó, M. Taravillo, V.G. Baonza, J.M. Recio, Phys. Chem. Chem. Phys. 21 (2019) 12585–12596.

[11] H.H. Osman, F.J. Manjón, Phys. Chem. Chem. Phys. 24 (2022) 9936–9942.

[12] Y. Cheng, S. Wahl, M. Wuttig, Phys. Status Solidi Rapid Res Lett. 15 (2021) 2000482.

[13] M. Wuttig, V.L. Deringer, X. Gonze, C. Bichara, J.-Y. Raty, Adv. Mater. 30 (2018) 1803777.

[14] M. Wuttig, N. Yamada, Nat. Mater. 6 (2007) 824–832.

[15] S. Raoux, F. Xiong, M. Wuttig, E. Pop, MRS Bull. 39 (2014) 703.

[16] S. Raoux, Annu. Rev. Mater. Res. 39 (2009) 25–48.

[17] K. Pielichowska, K. Pielichowski, Prog. Mater. Sci. 65 (2014) 67–123.

[18] M.Z. Hasan, C.L. Kane, Rev. Mod. Phys. 82 (2010) 3045–3067.

[19] I.T. Witting, T.C. Chasapis, F. Ricci, M. Peters, N.A. Heinz, G. Hautier, G.J. Snyder, Adv. Electron. Mater. 5 (2019) 1800904.

[20] Y. Yu, M. Cagnoni, O. Cojocaru-Mirédin, M. Wuttig, Adv. Funct. Mater. 30 (2020) 1904862.

[21] H. Krebs, Z. Elektrochem. Ber. Bunsenges. Phys. 61 (1957) 925–934.

[22] H. Krebs, Acta Cryst. 9 (1956) 95–108.

[23] G. Lucovsky, R.M. White, Phys. Rev. B 8 (1973) 660–667.

[24] P.B. Littlewood, Crit. Rev. Solid State Mater. Sci. 11 (1983) 229–285.

[25] L. Pauling, Phys. Rev. 54 (1938) 899–904.

[26] L. Pauling, Proc. R. Soc. Lond. A 196 (1949) 343–362.

[27] L. Pauling, The Nature of the Chemical Bond and the Structure of Molecules and Crys-Tals: An Introduction to Modern Structural Chemistry, Cornell Univ. Press, Ithaca, New York, 1960.

[28] W. Kutzelnigg, Angew. Chem. Int. Ed. Engl. 23 (1984) 272–295.

[29] M.L. Munzarová, R. Hoffmann, J. Am. Chem. Soc. 124 (2002) 4787–4795.

[30] U. V Waghmare, N.A. Spaldin, H.C. Kandpal, R. Seshadri, Phys. Rev. B 67 (2003) 125111.

[31] J.C. Golden, V. Ho, V. Lubchenko, J. Chem. Phys. 146 (2017) 174502.

[32] D.-K. Seo, R. Hoffmann, J. Solid State Chem. 147 (1999) 26–37.

[33] A. Ienco, R. Hoffmann, G. Papoian, J. Am. Chem. Soc. 123 (2001) 2317–2325.

[34] J.-Y. Raty, M. Schumacher, P. Golub, V.L. Deringer, C. Gatti, M. Wuttig, Adv. Mater. 31 (2019) 1806280.

[35] R.O. Jones, J. Phys.: Condens. Matter 30 (2018) 153001.

[36] R.O. Jones, J. Phys.: Condens. Matter 34 (2022) 343001.

[37] A. V Kolobov, P. Fons, J. Tominaga, S.R. Ovshinsky, Phys. Rev. B 87 (2013) 165206.

[38] A. V Kolobov, P. Fons, J. Tominaga, Sci. Rep. 5 (2015) 13698.

[39] J. Hempelmann, P.C. Müller, C. Ertural, R. Dronskowski, Angew. Chem. Int. Ed. 61 (2022) e202115778.

[40] P.C. Müller, C. Ertural, J. Hempelmann, R. Dronskowski, J. Phys. Chem. C 125 (2021) 7959–7970.

[41] J. Hempelmann, P.C. Müller, P.M. Konze, R.P. Stoffel, S. Steinberg, R. Dronskowski, Adv. Mater. 33 (2021) 2100163.

[42] T.H. Lee, S.R. Elliott, Adv. Mater. 32 (2020) 2000340.

[43] T.H. Lee, S.R. Elliott, Phys. Status Solidi Rapid Res. Lett. 15 (2021) 2000516.

[44] T.H. Lee, S.R. Elliott, Nat. Commun. 13 (2022) 1458.

[45] R.J. Hach, R.E. Rundle, J. Am. Chem. Soc. 73 (1951) 4321–4324.

[46] G.C. Pimentel, J. Chem. Phys. 19 (1951) 446–448.

[47] H.A. Bent, Chem. Rev. 68 (1968) 587–648.

[48] J.I. Musher, Angew. Chem. Int. Ed. Engl. 8 (1969) 54–68.

[49] G. A. Landrum, N. Goldberg, R. Hoffmann, J. Chem. Soc., Dalton Trans. (1997) 3605.

[50] G.A. Landrum, R. Hoffmann, Angew. Chem. Int. Ed. 37 (1998) 1887–1890.

[51] G. A. Papoian, R. Hoffmann, Angew. Chem. Int. Ed. 39 (2000) 2408–2448.

[52] J.-P. Gaspard, Phys. Status Solidi Rapid Res. Lett. 16 (2022) 2200111.

[53] R.F.W. Bader, Atoms in Molecules: A Quantum Theory, Clarendon Press, Oxford, 1990.

[54] R.L. DeKock, W.B. Bosma, J. Chem. Educ. 65 (1988) 194.

[55] F. Hund, Z. Phys. 51 (1928) 759–795.

[56] F. Bloch, Z. Phys. 52 (1929) 555–600.

[57] E. Hückel, Z. Phys. 70 (1931) 204–286.

[58] M. Wuttig, C.-F. Schön, J. Lötfering, P. Golub, C. Gatti, J.-Y. Raty, Adv. Mater. 35 (2023) 2208485.

[59] R.O. Jones, S.R. Elliott, R. Dronskowski, Adv. Mater. 35 (2023) 2300836.

[60] S. Shaik, D. Danovich, J.M. Galbraith, B. Braïda, W. Wu, P.C. Hiberty, Angew. Chem. Int. Ed. 59 (2020) 984–1001.

[61] S.P. Gnanasekar, E. Arunan, Aust. J. Chem. 73 (2020) 767–774.

[62] K. Wade, Electron Deficient Compounds, Nelson, London, 1971.

[63] C. Zheng, R. Hoffmann, Z. Naturforsch. B 41 (1986) 292–320.

[64] Á. Vegas, Structural Models of Inorganic Crystals, 1st ed., Universitat Politècnica de València, 2018.

[65] D. Lencer, M. Salinga, B. Grabowski, H. Tilmannand, J. Neugebauer, M. Wuttig, Nat. Mater. 7 (2008) 972–977.

[66] B. Huang, J. Robertson, Phys. Rev. B 81 (2010) 81204.

[67] M. Esser, S. Maintz, R. Dronskowski, J. Comput. Chem. 38 (2017) 620–628.

[68] Y. Cheng, O. Cojocaru-Mirédin, J. Keutgen, Y. Yu, M. Küpers, M. Schumacher, P. Golub, J.-Y. Raty, R. Dronskowski, M. Wuttig, Adv. Mater. 31 (2019) 1904316.

[69] L. Guarneri, S. Jakobs, A. von Hoegen, S. Maier, M. Xu, M. Zhu, S. Wahl, C. Teichrib, Y. Zhou, O. Cojocaru-Mirédin, M. Raghuwanshi, C.-F. Schön, M. Drögeler, C. Stampfer, R.P.S.M. Lobo, A. Piarristeguy, A. Pradel, J.-Y. Raty, M. Wuttig, Adv. Mater. 33 (2021) 2102356.

[70] K. Shportko, S. Kremers, M. Woda, L. Dominicand, J. Robertson, M. Wuttig, Nat. Mater. 7 (2008) 653–658.

[71] M. Wuttig, Phys. Status Solidi B 249 (2012) 1843–1850.

[72] N.W. Alcock, in: H.J. Emeléus, A.G. Sharpe (Eds.), Advances in Inorganic Chemistry and Radiochemistry, Academic Press, 1972, pp. 1–58.

[73] T. Clark, M. Hennemann, J.S. Murray, P. Politzer, J. Mol. Model. 13 (2007) 291–296.

[74] J.S. Murray, P. Lane, T. Clark, P. Politzer, J. Mol. Model. 13 (2007) 1033–1038.

[75] A. Varadwaj, P.R. Varadwaj, H.M. Marques, K. Yamashita, Molecules 27 (2022) 3421.

[76] S.J. Grabowski, Phys. Chem. Chem. Phys. 15 (2013) 7249–7259.

[77] S.J. Grabowski, Sci 4 (2022) 17.

[78] B. Silvi, E. Alikhani, H. Ratajczak, J. Mol. Model. 26 (2020) 62.

[79] S.J. Grabowski, Molecules 26 (2021) 4939.

[80] D.K. Miller, I.Yu. Chernyshov, Y. V Torubaev, S. V Rosokha, Phys. Chem. Chem. Phys. 24 (2022) 8251–8259.

[81] R.H. Crabtree, Chem. Soc. Rev. 46 (2017) 1720–1729.

[82] M.C. Aragoni, M. Arca, F.A. Devillanova, A. Garau, F. Isaia, V. Lippolis, A. Mancini, Bioinorg. Chem. Appl. 2007 (2007) 17416.

[83] M. Savastano, Dalton Trans. 50 (2021) 1142–1165.

[84] M. Xu, S. Jakobs, R. Mazzarello, J.-Y. Cho, Z. Yang, H. Hollermann, D. Shang, X. Miao, Z. Yu, L. Wang, M. Wuttig, J. Phys. Chem. C 121 (2017) 25447–25454.

[85] A. Pawbake, C. Bellin, L. Paulatto, K. Béneut, J. Biscaras, C. Narayana, D.J. Late, A. Shukla, Phys. Rev. Lett. 122 (2019) 145701.

[86] C. Bellin, A. Pawbake, L. Paulatto, K. Béneut, J. Biscaras, C. Narayana, A. Polian, D.J. Late, A. Shukla, Phys. Rev. Lett. 125 (2020) 145301.

[87] V.P. Cuenca-Gotor, J.Á. Sans, O. Gomis, A. Mujica, S. Radescu, A. Muñoz, P. Rodríguez-Hernández, E.L. da Silva, C. Popescu, J. Ibañez, R. Vilaplana, F.J. Manjón, Phys. Chem. Chem. Phys. 22 (2020) 3352–3369.

[88] W. Grochala, R. Hoffmann, J. Feng, N.W. Ashcroft, Angew. Chem. Int. Ed. 46 (2007) 3620–3642.

[89] A. Zhugayevych, V. Lubchenko, J. Chem. Phys. 133 (2010) 234503.

[90] R. Hoffmann, Solids and Surfaces: A Chemist's View of Bonding in Extended Structures, Wiley-VCH, 1988.

[91] H.G. von Schnering, Angew. Chem. Int. Ed. 20 (1981) 33–51.

[92] M. Kastner, Phys. Rev. Lett. 28 (1972) 355–357.

[93] The hypothetical *sc* phase of Sb at HP (see discussion in Section 2 of ESI) has been suggested to feature either ERM or Resonant/Metavalent bonds in several papers (see Refs. 51, 68, 69, and 70). However, systematic studies of group-15 and -16 elemental families to prove the unconventional character of the bonds in the *sc* phase of the different elements, the nature of the bond and the mechanism of the bond transformation have never been performed to the best of our knowledge.

[94] H.J. Beister, K. Strössner, K. Syassen, Phys. Rev. B 41 (1990) 5535–5543.

[95] H.C. Hsueh, C.C. Lee, C.W. Wang, J. Crain, Phys. Rev. B 61 (2000) 3851–3856.

[96] J.-P. Gaspard, A. Pellegatti, F. Marinelli, C. Bichara, Philos. Mag. B 77 (1998) 727–744.

[97] J.-P. Gaspard, C. R. Phys. 17 (2016) 389–405.

[98] The above consideration is not surprising because the crystalline structures at RP of most group-15 and -16 elements as well as most IV-VI and V_2-VI_3 compounds feature a mixture of a primary covalent *ppσ*-bond and a secondary LEP-based bond [24, 120]. In addition, both group-15 and IV-VI compounds are all 10-electron materials [24].

[99] J.A. Sans, R. Vilaplana, E.L. da Silva, C. Popescu, V.P. Cuenca-Gotor, A. Andrada-Chacón, J. Sánchez-Benitez, O. Gomis, A.L.J. Pereira, P. Rodríguez-Hernández, A. Muñoz, D. Daisenberger, B. García-Domene, A. Segura, D. Errandonea, R.S. Kumar, O. Oeckler, P. Urban, J. Contreras-García, F.J. Manjón, Inorg. Chem. 59 (2020) 9900–9918.

[100] D. Cremer, E. Kraka, Angew. Chem. Int. Ed. Engl. 23 (1984) 627–628.

[101] O. Degtyareva, M.I. McMahon, R.J. Nelmes, High Press. Res. 24 (2004) 319–356.

[102] P. Silas, J.R. Yates, P.D. Haynes, Phys. Rev. B 78 (2008) 174101.

[103] C.R.S. da Silva, R.M. Wentzcovitch, Comput. Mater. Sci. 8 (1997) 219–227.

[104] D. Scelta, A. Baldassarre, M. Serrano-Ruiz, K. Dziubek, A.B. Cairns, M. Peruzzini, R. Bini, M. Ceppatelli, Angew. Chem. Int. Ed. 56 (2017) 14135–14140.

[105] D. Olego, M. Cardona, Phys. Rev. B 25 (1982) 1151–1160.

[106] T. Matsunaga, N. Yamada, R. Kojima, S. Shamoto, M. Sato, H. Tanida, T. Uruga, S. Kohara, M. Takata, P. Zalden, G. Bruns, I. Sergueev, H.C. Wille, R.P. Hermann, M. Wuttig, Adv. Funct. Mater. 21 (2011) 2232–2239.

[107] S. Lee, K. Esfarjani, T. Luo, J. Zhou, Z. Tian, G. Chen, Nat. Commun. 5 (2014) 3525.

[108] J.S. Lannin, J.M. Calleja, M. Cardona, Phys. Rev. B 12 (1975) 585–593.

[109] W. Richter, T. Fjeldly, J. Renucci, M. Cardona, In Proceedings of the International Conference on Lattice Dynamics, edited by M. Balkanski, Flammarion, Paris, 1978.

[110] R. Arora, U. V Waghmare, C.N.R. Rao, Adv. Mater. 35 (2023) 2208724.

[111] P. Mori-Sánchez, A.M. Pendás, V. Luaña, J. Am. Chem. Soc. 124 (2002) 14721–14723.

[112] A.M. Redon, J.M. Leger, High Press. Res. 4 (1990) 315–317.

[113] A. Onodera, I. Sakamoto, Y. Fujii, N. Môri, S. Sugai, Phys. Rev. B 56 (1997) 7935–7941.

[114] X. Wang, K. Kunc, I. Loa, U. Schwarz, K. Syassen, Phys. Rev. B 74 (2006) 134305.

[115] Y. Zhao, S. Clément, J. Haines, R. Viennois, J. Phys. Chem. C. 124 (2020) 26659–26669.

[116] E. Zahedi, B. Xiao, Comput. Mater. Sci. 101 (2015) 301–312.

[117] J. Ibáñez, J.A. Sans, C. Popescu, J. López-Vidrier, J.J. Elvira-Betanzos, V.P. Cuenca-Gotor, O. Gomis, F.J. Manjón, P. Rodríguez-Hernández, A. Muñoz, J. Phys. Chem. C 120 (2016) 10547–10558.

[118] M.I. McMahon, O. Degtyareva, R.J. Nelmes, Phys. Rev. Lett. 85 (2000) 4896–4899.

[119] H. Olijnyk, S. Nakano, K. Takemura, Phys. Status Solidi B 244 (2007) 3572–3582.

[120] A. von Hippel, J. Chem. Phys. 16 (1948) 372–380.

[121] O. Degtyareva, E. Gregoryanz, H.K. Mao, R.J. Hemley, High Press. Res. 25 (2005) 17–33.

[122] Y. Akahama, M. Kobayashi, H. Kawamura, Phys. Rev. B 47 (1993) 20–26.

[123] T. Krüger, W.B. Holzapfel, Phys. Rev. Lett. 69 (1992) 305–307.

[124] J.C. Jamieson, D.B. McWhan, J. Chem. Phys. 43 (1965) 1149–1152.

[125] G. Parthasarathy, W.B. Holzapfel, Phys. Rev. B 37 (1988) 8499–8501.

[126] C. Hejny, M.I. McMahon, Phys. Rev. Lett. 91 (2003) 215502.

[127] S. Minomura, K. Aoki, N. Koshizuka, T. Tsushima, The Effect of Pressure on The Raman Spectra in Trigonal Se and Te, (Eds: K. D. Timmerhaus, M. S. Barber), Springer US, Boston, MA, 1979.

[128] G. Parthasarathy, W.B. Holzapfel, Phys. Rev. B 38 (1988) 10105–10108.

[129] O. Yoshinori, Y. Itsuro, Y. Makoto, E. Hirohisa, J. Phys. Soc. Japan 64 (1995) 4766–4789.

[130] A.K. Bandyopadhyay, D.B. Singh, Pramana 52 (1999) 303–319.

[131] O. Degtyareva, E.R. Hernández, J. Serrano, M. Somayazulu, H. Mao, E. Gregoryanz, R.J. Hemley, J. Chem. Phys. 126 (2007) 84503.

[132] C. Marini, D. Chermisi, M. Lavagnini, D. Di Castro, C. Petrillo, L. Degiorgi, S. Scandolo, P. Postorino, Phys. Rev. B 86 (2012) 64103.

[133] X. Li, X. Huang, X. Wang, M. Liu, G. Wu, Y. Huang, X. He, F. Li, Q. Zhou, B. Liu, T. Cui, Phys. Chem. Chem. Phys. 20 (2018) 6116–6120.

[134] Y. Akahama, M. Kobayashi, H. Kawamura, Solid State Commun. 84 (1992) 803–806.

[135] J.-Y. Raty, C. Gatti, C.-F. Schön, M. Wuttig, Phys. Status Solidi RRL 15 (2021) 2000534.

[136] Y. Akahama, M.K.M. Kobayashi, H.K.H. Kawamura, Jpn. J. Appl. Phys. 31 (1992) L1621.

[137] U. Häussermann, K. Söderberg, R. Norrestam, J. Am. Chem. Soc. 124 (2002) 15359–15367.

[138] M. Zhu, O. Cojocaru-Mirédin, A.M. Mio, J. Keutgen, M. Küpers, Y. Yu, J.-Y. Cho, R. Dronskowski, M. Wuttig, Adv. Mater. 30 (2018) 1706735.

[139] P. Bauer Pereira, I. Sergueev, S. Gorsse, J. Dadda, E. Müller, R.P. Hermann, Phys. Status Solidi B 250 (2013) 1300–1307.

[140] R. Dronskowski, P.E. Bloechl, J. Phys. Chem. 97 (1993) 8617–8624.

[141] V.L. Deringer, R.P. Stoffel, M. Wuttig, R. Dronskowski, Chem. Sci. 6 (2015) 5255–5262.

[142] S. Deng, J. Köhler, A. Simon, Angew. Chem. Int. Ed. 45 (2006) 599–602.

[143] B. Silvi, J. Mol. Struct. 614 (2002) 3–10.

[144] R. Hoffmann, J.M. Howell, E.L. Muetterties, J. Am. Chem. Soc. 94 (1972) 3047–3058.

[145] M.M.L. Chen, R. Hoffmann, J. Am. Chem. Soc. 98 (1976) 1647–1653.

[146] T. Masaharu, N. Kiyofumi, J. Phys. Soc. Japan 76 (2007) 17–18.

[147] V. Labet, R. Hoffmann, N.W. Ashcroft, J. Chem. Phys. 136 (2012) 074503.

[148] V. Labet, R. Hoffmann, N.W. Ashcroft, J. Chem. Phys. 136 (2012) 074502.

[149] V. Labet, P. Gonzalez-Morelos, R. Hoffmann, N.W. Ashcroft, J. Chem. Phys. 136 (2012) 074501.

[150] V. Riffet, V. Labet, J. Contreras-García, Phys. Chem. Chem. Phys. 19 (2017) 26381–26395.

[151] A. Mujica, A. Rubio, A. Muñoz, R.J. Needs, Rev. Mod. Phys. 75 (2003) 863–912.

[152] B.A. Weinstein, G.J. Piermarini, Phys. Rev. B 12 (1975) 1172–1186.

[153] R.M. Martin, T.A. Fjeldly, W. Richter, Solid State Commun. 18 (1976) 865–869.

[154] R.M. Martin, G. Lucovsky, K. Helliwell, Phys. Rev. B 13 (1976) 1383–1395.

[155] K.J. Chang, M.L. Cohen, Phys. Rev. B 33 (1986) 7371–7374.

[156] A. Minelli, S.M. Souliou, T. Nguyen-Thanh, A.H. Romero, J. Serrano, W.I. Hernandez, M.J. Verstraete, V. Dmitriev, A. Bosak, Phys. Rev. B 100 (2019) 104305.

[157] B.A. Weinstein, Phys. Rev. B 104 (2021) 54105.

[158] M.H. Cohen, L.M. Falicov, S. Golin, IBM J. Res. Dev. 8 (1964) 215–227.

[159] J.F. Khoury, L.M. Schoop, Trends Chem 3 (2021) 700–715.

[160] L.A. Agapito, N. Kioussis, W.A. Goddard, N.P. Ong, Phys. Rev. Lett. 110 (2013) 176401.

[161] W. Richter, J.B. Renucci, M. Cardona, Phys. Status Solidi B 56 (1973) 223–229.

[162] A. Katsutoshi, S. Osamu, M. Shigeru, K. Naoki, T. Tachiro, J. Phys. Soc. Japan 48 (1980) 906–911.

[163] J. Contreras-García, Á.M. Pendás, B. Silvi, J.M. Recio, J. Phys. Chem. B 113 (4) (2009) 1068–1073.

[164] A.L.J. Pereira, J.A. Sans, R. Vilaplana, O. Gomis, F.J. Manjón, P. Rodríguez-Hernández, A. Muñoz, C. Popescu, A. Beltrán, J. Phys. Chem. C. 118 (2014) 23189–23201.

[165] C. Buzea, K. Robbie, Supercond. Sci. Technol. 18 (2004) R1.

[166] O. Prakash, A. Kumar, A. Thamizhavel, S. Ramakrishnan, Science (1979) 355 (2017) 52–55.

[167] R.O. Jones, Phys. Rev. B 101 (2020) 24103.

[168] I. Mayer, J. Mol. Struct.: THEOCHEM 186 (1989) 43–52.

[169] M.J. Molina, J.A. Dobado, Theor. Chem. Acc. 105 (2001) 328–337.

[170] M. Wuttig, C.-F. Schön, M. Schumacher, J. Robertson, P. Golub, E. Bousquet, C. Gatti, J.-Y. Raty, Adv. Funct. Mater. 32 (2022) 2110166.

[171] L.J. Sæthre, O. Gropen, J. Sletten, T. Pedersen, L.B. Zinner, F. Lehrich, C.J. Nielsen, D.L. Powell, M. Trætteberg, Acta Chem. Scand. 42a (1988) 16–26.

[172] W.H. Eberhardt, B. Crawford Jr., W.N. Lipscomb, J. Chem. Phys. 22 (1954) 989–1001.

[173] D. Akhtar, V.D. Vankar, T.C. Goel, K.L. Chopra, J. Mat. Sci. 14 (1979) 2422–2426.

[174] M. Brylak, M.H. Möller, W. Jeitschko, J. Solid State Chem. 115 (1995) 305–308.

[175] R. Nesper, Prog. Solid. State Ch. 20 (1990) 1–45.

[176] In the *I4/mmm* structure of $BaZnSb_2$ there are two different Wyckoff sites for Sb atoms (*4c* and *4e* sites). Each independent Sb atom has a different charge.

[177] P. Böttcher, Angew. Chem. Int. Ed. 27 (1988) 759–772.

[178] A.L. de J. Pereira, D. Santamaría-Pérez, R. Vilaplana, D. Errandonea, C. Popescu, E.L. da Silva, J.A. Sans, J. Rodríguez-Carvajal, A. Muñoz, P. Rodríguez-Hernández, A. Mujica, S.E. Radescu, A. Beltrán, A. Otero-de-la-Roza, M. Nalin, M. Mollar, F.J. Manjón, Inorg. Chem. 59 (2020) 287–307.

[179] S.J. Grabowski, Phys. Chem. Chem. Phys. 19 (2017) 29742–29759.

[180] G. Parkin, J. Chem. Educ. (2023).

[181] K.S. Pitzer, J. Am. Chem. Soc. 67 (1945) 1126–1132.

[182] G. Parkin, J. Chem. Educ. 96 (2019) 2467–2475.

[183] G.R. Eaton, Found. Chem. 25 (2023) 285–298.

[184] A.D. Walsh, Journal of the Chemical Society (Resumed) (1947) 89.

[185] T. Poręba, S. Racioppi, G. Garbarino, W. Morgenroth, M. Mezouar, Inorg. Chem. 61 (2022) 10977–10985.

[186] J. Möbs, G. Stuhrmann, F. Weigend, J. Heine, Chem. Eur. J. 29 (2023) e202202931.

[187] S. Hayashi, T. Nishide, W. Nakanishi, Heter. Chem. 29 (2018) 1–12.

[188] D. Hirai, K. Kojima, N. Katayama, M. Kawamura, D. Nishio-Hamane, Z. Hiroi, J. Am. Chem. Soc. 144 (2022) 17857–17864.

[189] K. Raghavachari, P. von R. Schleyer, G.W. Spitznagel, J. Am. Chem. Soc. 105 (1983) 5917–5918.

[190] A.M. Sapse, L. Osorio, Inorg. Chem. 23 (1984) 627–628.

[191] H.G. Grimm, A. Sommerfeld, Z. Physik 36 (1926) 36–59.

[192] W. Hume-Rothery, Phil. Mag. S. 9 (1930) 65–80.

[193] W.B. Pearson, Acta Cryst. 17 (1964) 1–15.

[194] S. Noury, B. Silvi, R.J. Gillespie, Inorg. Chem. 41 (2002) 2164–2172.

[195] G.N. Lewis, J. Am. Chem. Soc. 38 (1916) 762–785.

[196] P. von R. Schleyer, Chem. Eng. News 62 (1984) 4.

[197] L. Suidan, J.K. Badenhoop, E.D. Glendening, F. Weinhold, J. Chem. Educ. 72 (1995) 583.

[198] O.J. Curnow, J. Chem. Educ. 75 (1998) 910.

[199] W.B. Jensen, J. Chem. Educ. 83 (2006) 1751.

[200] J.M. Galbraith, J. Chem. Educ. 84 (2007) 783.

[201] B.A. Jackson, J. Harshman, E. Miliordos, J. Chem. Educ. 97 (2020) 3638–3646.

[202] N.C. Norman, P.G. Pringle, Chemistry (Easton) 4 (2022) 1226–1249.

[203] R.J. Gillespie, R.S. Nyholm, Q. Rev. Chem. Soc. 11 (1957) 339–380.

[204] A. Åström, S. Andersson, J. Solid State Chem. 6 (1973) 191–194.

[205] M. Bykov, E. Bykova, M. Hanfland, H. Liermann, R.K. Kremer, R. Glaum, L. Dubrovinsky, S. van Smaalen, Angew. Chem. Int. Ed. 55 (2016) 15053–15057.

[206] J. Pilmé, E.A. Robinson, R.J. Gillespie, Inorg. Chem. 45 (2006) 6198–6204.

[207] E.O. Gomes, A.F. Gouveia, L. Gracia, Á. Lobato, J.M. Recio, J. Andrés, J. Phys. Chem. Lett. 13 (2022) 9883–9888.

[208] H. Iwasaki, T. Kikegawa, Acta. Cryst. B 53 (1997) 353–357.

[209] D. Laniel, B. Winkler, T. Fedotenko, A. Pakhomova, S. Chariton, V. Milman, V. Prakapenka, L. Dubrovinsky, N. Dubrovinskaia, Phys. Rev. Lett. 124 (2020) 216001.

[210] A. Walsh, G.W. Watson, J. Phys. Chem. B 109 (2005) 18868–18875.

[211] A. Liang, S. Rahman, P. Rodriguez-Hernandez, A. Muñoz, F.J. Manjón, G. Nenert, D. Errandonea, J. Phys. Chem. C 124 (2020) 21329–21337.

[212] A. Liang, C. Popescu, F.J. Manjon, P. Rodriguez-Hernandez, A. Muñoz, Z. Hebboul, D. Errandonea, Phys. Rev. B 103 (2021) 054102.

[213] B.B. Sharma, P.S. Ghosh, A.K. Mishra, H.K. Poswal, Vib. Spectrosc. 117 (2021) 103318.